

Accepted for publication on the Astrophysical Journal

Systematic Investigation of Solar Modulation of Galactic Protons for Solar Cycle 23 using a Monte Carlo Approach with Particle Drift Effects and Latitudinal Dependence

P. Bobik¹, G. Boella^{2,3}, M.J. Boschini^{2,4}, C. Consolandi², S. Della Torre^{2,5}, M. Gervasi^{2,3}, D. Grandi², K. Kudela¹, S. Pensotti^{2,3}, P.G. Rancoita² and M. Tacconi²

Istituto Nazionale di Fisica Nucleare, INFN, Milano-Bicocca, Milano (Italy), I20126

piergiorgio.rancoita@mib.infn.it

ABSTRACT

A propagation model of galactic cosmic protons through the Heliosphere was implemented using a 2-D Monte Carlo approach to determine the differential intensities of protons during the solar cycle 23. The model includes the effects due to the variation of solar activity during the propagation of cosmic rays from the boundary of the heliopause down to Earth's position. Drift effects are also accounted for. The simulated spectra were found in agreement with those obtained with experimental observations carried out by BESS, AMS and PAMELA collaborations. In addition, the modulated spectrum determined with the present code for the year 1995 exhibits the latitudinal gradient and equatorial southward offset minimum found by Ulysses fast scan in 1995.

Subject headings: Solar modulation, Interplanetary space, Cosmic rays propagation

¹Institute of Experimental Physics, Kosice (Slovak Republic).

²INFN, Milano-Bicocca, Milano (Italy).

³also Physics Department, University of Milano-Bicocca, Milano (Italy).

⁴also CILEA, Segrate (Milano, Italy).

⁵also University of Insubria, Como (Italy).

1. Introduction

During the last two decades - using balloon flights and space-borne missions -, the fluxes of Galactic Cosmic Rays (GCR) and their energy distributions were observed in different phases of solar activity. These data allow one to attempt a better understanding of processes related to the transport of GCRs through the Heliosphere. Furthermore, the study of propagation properties - i.e., the effect of solar modulation on the fluxes - of GCRs may, in turn, provide a tool to determine demodulated Local Interstellar Spectra (LIS) of GCR components, for instance, protons, light-nuclei, electrons, positrons, anti-protons, etc., thus, a further understand of processes of generation, acceleration and diffusion within the Milky Way (e.g., see Boella et al. 1998; Strong et al. 2007; Evoli et al. 2008; Putze et al. 2009). In addition, an accurate determination of demodulated spectra may allow one to untangle features due to new physics - i.e., dark matter (e.g., see Bottino et al. 1998; Cirelli & Cline 2010; Ibarra et al. 2010; Salati 2011; Weniger 2011, and references therein) - or astrophysical sources (e.g., see Chang et al. 2008; Abdo et al. 2009; Adriani et al. 2009a; Cernuda 2011; Mertsch & Sarkar 2011, and references therein).

Recently, spectra of GCRs were obtained using dedicated spectrometers on space born-missions (e.g., see Alcaraz et al. 2000a,b,c,d; Aguilar et al. 2002, 2007; Adriani et al. 2009a,b, 2010) and balloon flights (e.g., see Boezio et al. 1999; Menn et al. 2000; Haino et al. 2004; Shikaze et al. 2007; Abe et al. 2008; Mitchell et al. 2008). These spectra were measured i) with an accuracy down to about or less than 30% and ii) covering a time duration longer than a solar cycle, i.e., these spectra were measured under solar conditions largely different. These data can be hopefully exploited to determine a general treatment of solar modulation in the inner heliosphere to be used for different phases of solar activity and a better understanding of space radiation environment close to Earth (e.g., see Leroy & Rancoita 2007, and references therein). In the near future even more accurate and systematic data will be available from AMS-02. This spectrometer is operational onboard of the International Space Station from May 2011 and is expected to collect data for more than a solar cycle (Battiston 2010; Bobik et al. 2010a). These observations will allow one to obtain accurate spectra with different solar activity conditions from some hundreds MeV up to very high energy (a few TeV's); in addition, using the same experimental apparatus, systematic errors on measured fluxes are expected to be minimized. Furthermore, observations made by the Ulysses spacecraft (Simpson et al. 1992) in the inner heliosphere could determine a latitudinal dependence of GCR (mostly protons) intensity with an equatorial southward offset minimum and a North polar excess (e.g., see Simpson, Zhang and Bame 1996). Finally, it has be remarked that modulation phenomena were observed at low energies (i.e., lower than 500 MeV/nucleon) in the outer heliosphere (e.g., see Webber et al. 2008) and are currently investigated, for instance, by Langner et al. (2003); Langner & Potgieter (2004); Bobik et al. (2008b); Potgieter (2008)

(see also references therein).

In the present model, a two dimensional (2-D) - i.e., depending on the helio-colatitude and radial distance from the Sun (Bobik et al. 2003, 2008, 2010a) - Monte Carlo approach is adopted to solve the transport equation of propagation of GCRs down to the inner heliosphere, without addressing CR modulation observed in the outer. The model exhibits a slow time dependence because of the (almost) monthly averages of solar activity parameters adopted for the i) solar wind speed (V_{sw}), ii) tilt angle (α_t) of the neutral sheet and iii) diffusion parameter K_0 (discussed in Sect. 2.1). Furthermore, one has to remark that the solar wind usually takes of the order of or more than one year to reach the border of the heliosphere. As a consequence, the above parameters are locally evaluated within the heliosphere, allowing the modulation treatment to better (or *dynamically*) account for the effects of solar activity as a function of the distance from the Sun. In addition, the current treatment accounts for effects due to the charge sign of particles (i.e., the so-called *particle drift effect*), e.g., those related, for instance, to a) the curvature and gradient of the interplanetary magnetic field (IMF) and b) the extension of the neutral current sheet inside the heliosphere. Thus the model introduces a dependence on the sign solar-field polarity (A) (e.g., see Clem et al. 1996; Boella et al. 2001). The present code allows the fluxes of protons (as well antiprotons) and helium nuclei to be modulated from the border of the heliosphere down to Earth - but outside Earth's magnetosphere (Bobik et al. 2006) - in order to compare them with the available experimental observations. Furthermore, electrons and positrons modulated spectra can be derived accounting for the additional collision, radiative and inverse Compton energy-losses (see Bobik et al. 2011c).

In the next sections, the heliosphere, drifts, diffusion tensor, determination of the diffusion parameter, dependence of both the solar wind and IMF on the radial distance and helio-colatitude, neutral current sheet are discussed (Sects. 2–4). Then, the implementation of the mathematical model and the parametrization with the dynamical treatment of heliosphere are treated (Sects. 5, 6). Finally, comparisons among obtained modulated spectra of differential intensities with those experimentally observed are performed and discussed (Sects. 7–7.4).

2. Heliosphere and Drift Mechanisms

The transport of galactic protons (GP) inside the heliosphere was initially treated by Parker (1965), who demonstrated that - in the framework of statistical physics - the random walk of the cosmic ray particles is a Markoff process, describable by a Fokker–Planck equation (hereafter FPE) (e.g., see also Axford 1965; Fisk 1976; Potgieter et al. 1993, and

also Sections 4.1.2.4 of Leroy & Rancoita 2011, and references therein). Thus (at the time t), the number density¹ U of GPs per unit interval of particle kinetic energy T (the so-called differential density) can be obtained from the solution of the FPE:

$$\frac{\partial U}{\partial t} = \frac{\partial}{\partial x_i} \left(K_{ij}^S \frac{\partial U}{\partial x_j} \right) + \frac{1}{3} \frac{\partial V_{sw,i}}{\partial x_i} \frac{\partial}{\partial T} (\alpha_{rel} T U) - \frac{\partial}{\partial x_i} (V_{sw,i} U) - \frac{\partial}{\partial x_i} (v_{d,i} U) \quad (1)$$

(e.g., see Jokipii et al. 1977, Equation (4.75) in Section 4.1.2.6 of Leroy & Rancoita 2011 and references therein) with $V_{sw,i}$ the solar wind velocity along the axis x_i ,

$$v_{d,i} = \frac{\partial K_{ij}^A}{\partial x_j} \quad (2)$$

the drift velocity (e.g., see Jokipii et al. 1977; Jokipii & Levy 1977 and also Bobik et al. 2010b and references therein), K_{ij}^A and K_{ij}^S the antisymmetric and symmetric part of the diffusion tensor - respectively -,

$$\alpha_{rel} = \frac{T + 2m_r c^2}{T + m_r c^2}$$

and m_r the rest mass of the proton. The number density U is related to the differential intensity J as:

$$J = \frac{v U}{4\pi}, \quad (3)$$

where v is the speed of the GCR particle. Equation (1) - as well known - describes i) the diffusion of GCRs by magnetic irregularities, ii) the so-called *adiabatic-energy changes* associated with expansions and compressions of cosmic radiation, iii) the convection effect resulting from the solar wind with velocity \vec{V}_{sw} and iv) the drift effects related to the *drift velocity* (\vec{v}_d). In turn, the drift velocity is determined by the antisymmetric part of the diffusion tensor [see Eq. (2) and Sect. 4] which accounts for gradient, curvature and current sheet drifts of particles in the IMF, i.e., it depends on the charge sign of particles.

Furthermore - as discussed by Jokipii & Levy (1977) -, one can re-write Eq.(1) as

$$\frac{\partial U}{\partial t} = \frac{\partial}{\partial x_i} \left(K_{ij}^S \frac{\partial U}{\partial x_j} \right) + \frac{1}{3} \frac{\partial V_{sw,i}}{\partial x_i} \frac{\partial}{\partial T} (\alpha_{rel} T U) - \frac{\partial}{\partial x_i} [(V_{sw,i} + v_{d,i}) U]. \quad (4)$$

Thus, one obtains that drift effects are accounted for by a convection velocity in which the drift velocity is added to the solar wind velocity. In this way, the resulting *effective convection*

¹The equivalent expression in terms of the omnidirectional distribution function of CR particles with momentum \vec{p} , at the position \vec{r} and time t can be found, for instance, expressed in Equation (1) of Potgieter (1998) (see also references therein).

velocity may non-negligibly differ from that due to the solar wind; but - as remarked by Jokipii & Levy (1977) - noting that $\nabla \cdot \vec{v}_d = 0$, one finds that drift effects do not contribute to the adiabatic-energy changes [second right-hand term of Eqs. (1, 4)]. Even if drift effects are included² in Eqs. (1, 4), some modulation models³ neglected it (e.g., see Jokipii et al. 1977; Usoskin et al. 2005, and references therein). Gradients of particle density can also result from the convection effect. Drift mechanisms can modify both the radial and (solar) latitude dependence of the gradient magnitude. For instance, drift motions can affect modulated GCR spectra by redirecting particles within the heliosphere (Jokipii et al. 1977). When the particle Larmor radius is much shorter than the magnetic-field scale length, drift effects can be taken into account by evaluating the average distance in which a relevant field variation occurs. Drift effects affect particle motions over large distances due to the large scale variation of the IMF strength. Different intensities of GCR modulation were observed in time periods with opposite field polarity, for instance, by Emerson & Meyer (1984); Garcia-Munoz et al. (1986); Clem et al. (2000); Boella et al. (2001). Thus, it is necessary to explicitly consider particle drifts inside the equation of propagation of GCR.

As well known for a reference system with the 3rd coordinate along the average magnetic field, the symmetric part of the diffusion tensor (or coefficient) - for an isotropic perpendicular diffusion - includes both the transverse (K_{\perp}) and parallel (K_{\parallel}) components (e.g., see Jokipii 1971; Potgieter & Moraal 1985; Potgieter & Le Roux 1994). In turn, for a standard Parker field [Eq. (15)] these two components are related to the radial component in heliocentric spherical coordinates as

$$K_{rr} = K_{\parallel} \cos^2 \psi + K_{\perp} \sin^2 \psi, \quad (5)$$

with ψ the angle between radial and magnetic field directions - the so-called *spiral angle* [Eq. (16)] - (e.g., see Fisk 1976; Potgieter & Le Roux 1994) and $K_{\theta\theta} = K_{\perp}$, where θ is the polar angle (Potgieter et al. 1993). It has to be remarked that the general transformations of the symmetric and antisymmetric parts of the diffusion tensor from field-aligned to heliospheric (spherical) coordinates can be found in (Burger et al. 2008). Furthermore, it has to be remarked that a general discussion about the role of parallel and perpendicular diffusion is available in Giacalone & Jokipii 1999.

Potgieter & Le Roux (1994) (see also Potgieter et al. 1993) suggested that the parallel

²One can see the discussions in (Parker 1965; Jokipii & Parker 1970; Jokipii & Levy 1977; Jokipii et al. 1977; Potgieter 1998).

³Like, for instance, the so-called *force-field model* (FFM) (see Gleeson & Axford 1968).

diffusion coefficient is given by

$$K_{\parallel} \approx \beta k_1(r, t) K_P(P, t) \left[\frac{B_{\oplus}}{3B} \right] \quad (6)$$

with $\beta = v/c$, v the particle velocity and c the speed of light; the diffusion parameter k_1 accounts for the dependence on the solar activity and is treated in Sect. 2.1; B_{\oplus} (typically ≈ 5 nT) is the value of IMF at Earth’s orbit but it varies as a function of the time; B is the magnitude of the large scale IMF (discussed in Sect. 3), thus, it depends on the heliospheric region (Sect. 5) through which GCRs are transported; finally, the term K_P takes into account the dependence on the rigidity P of the GCR particle and is usually expressed in GV. To a first approximation, one can assume that

$$K_P \approx P \quad (7)$$

for particle rigidities above a threshold value P_{th} within the rigidity range (0.4–1.015) GV, as commonly supposed by many authors (e.g., see Gloeckler & Jokipii 1966; Gleeson & Axford 1968; Perko 1987; Potgieter & Le Roux 1994; Strauss et al. 2011). In the present model, K_P is assumed to be equal to the value of the rigidity (P) above the upper limit of the P_{th} range, i.e., for proton kinetic energies $\gtrsim 0.444$ GeV (see Sects. 7.2, 7.2.1). Below P_{th} , it can be usually approximated to a constant (e.g., see Perko 1987; Potgieter & Le Roux 1994; Wibberenz et al. 2001; Strauss et al. 2011). It has to be remarked that nowadays treatments resulting in a more complex dependence of the diffusion tensor on rigidity are proposed by several authors (e.g., see Ferreira et al. 2001; Pei et al. 2010a, and references therein). Some of these studies are motivated from dealing with magnetohydrodynamic turbulence in the expanding solar wind and/or accounting observations carried out on data of low energy electrons collected using spacecrafts [for instance, (3–10) MeV from Ulysses spacecraft in (Ferreira et al. 2001) and 16 MeV from Pioneer 10 in (Potgieter & Ferreira 2002)].

In heliocentric spherical coordinates, the perpendicular diffusion coefficient has two components, one along the radial direction, $K_{\perp r}$, the other one for the polar direction $K_{\perp \theta}$. ρ_k is the ratio between perpendicular (in the radial direction) and parallel diffusion coefficients, i.e., $K_{\perp r} = \rho_k K_{\parallel}$. In the present model, we use $\rho_k = 0.05$: this value is in the mid of the range suggested by Palmer (1982) (see also Giacalone 1998 and Section 6.3 of Burger et al. 2000). The value of the perpendicular diffusion coefficient in the polar direction ($K_{\perp \theta}$) can be assumed to be almost equal to that radial ($K_{\perp r}$) (e.g., see Potgieter 2000, and references therein). However, Potgieter (2000) suggested the usage of an *enhanced* $K_{\perp \theta}$ in the polar regions in order to reproduce the amplitude and rigidity dependence of the latitudinal gradients of GCR differential intensities for protons and electrons (e.g., see

Potgieter 1997; Heber et al. 1998). He introduced a sharp transition (via a transition function, e.g., see Figure 7 in that article) in the colatitude regions $120^\circ \lesssim \theta \lesssim 130^\circ$ and $60^\circ \gtrsim \theta \gtrsim 50^\circ$. He also derived that $K_{\perp\theta}$ has to be increased by a factor of about (or larger than) 10; Ferreira & Potgieter (2004) used a factor of 8. In the current code, $K_{\perp\theta}$ is given by:

$$K_{\perp\theta} = \begin{cases} 10 K_{\perp r}, & \text{in the polar regions,} \\ K_{\perp r}, & \text{in the equatorial region,} \end{cases} \quad (8)$$

where the polar regions correspond to colatitudes with $\theta \lesssim 30^\circ$ or $\theta \gtrsim 150^\circ$, while the equatorial region corresponds to colatitudes with $30^\circ \lesssim \theta \lesssim 150^\circ$. The solar colatitudes of 30° and 150° correspond to those at which the SW speed becomes constant in periods not dominated by high solar activity [Eq. (17)]. The usage of the transition function can be fully implemented in current treatment, but is not required with the present overall code accuracy. In fact, the results obtained from the so-called “L” *model* (i.e., the one with a better agreement with data, see Sects. 7.2, 7.2.1) indicate that only in periods not dominated by high solar activity the enhancement of $K_{\perp\theta}$ [Eq. (8)] slightly improve the overall agreement with data by a few percent. Finally, in Appendix A the diffusion coefficients in heliocentric polar coordinates are expressed in terms of those parallel and perpendicular to the IMF.

Moreover, it has to be remarked that the diffusion tensor i) is not well determined during solar maxima and ii) can be adapted to better account for the complex structure of the IMF - which depends on the solar activity - found with Ulysses spacecraft (e.g., see Burger et al. 2008, and references therein). For instance, Potgieter, Burger and Ferreira (2001) - see also references therein - discussed the so-called *propagating diffusion barriers* and suggested a time dependent model for the diffusion coefficients. The latter are supposed to be $\propto [B_0/B(t)]^n$, where $B(t)$ is the IMF magnitude at the time t and $B_0 = 5$ nT is the average IMF magnitude during minimum modulation conditions at Earth (Potgieter & Ferreira 2001; Potgieter et al. 2003) and n is the ratio between the actual tilt-angle value (Sect. 3) and that close to solar minimum (7° – 15°) (e.g., see Potgieter & Ferreira 2001; Potgieter et al. 2001). However, in the current model the time dependence of diffusion coefficients is taken into account using a diffusion parameter, which is treated in Sect. 2.1. The agreement with data obtained during high solar activity is discussed in Sect. 7.2.

2.1. Diffusion Parameter in the Framework of the Force Field Model

In the FFM (e.g., see Gleeson & Axford 1968; Gleeson & Urch 1971 and also Section 4.1.2.4 of Leroy & Rancoita 2011), Gleeson & Axford (1968) assumed that, at the time

t , i) modulation effects can be expressed with a spherically symmetric modulated differential number density U of GCRs, ii) the diffusion coefficient reduces to a scalar⁴ given by a separable function of r (the radial distance from the Sun) and P (the particle rigidity in GV):

$$\mathcal{K}(r, t) = \beta k_1(r, t) K_P(P, t) \quad (9)$$

with K_P from Eq. (7) for particle rigidities above ≈ 1 GV, and iii) the modulation occurs in a steady-state condition, i.e., the relaxation time of the distribution is short with respect to the solar cycle duration so that one can assume that the partial derivative of U with respect to time is zero. They derived that the differential intensity [Eq. (3)] at a radial distance r is given by the expression

$$J(r, E_t, t) = J(r_{\text{tm}}, E_t + \Phi_p) \left[\frac{E_t^2 - m_r^2 c^4}{(E_t + \Phi_p)^2 - m_r^2 c^4} \right], \quad (10)$$

where $J(r_{\text{tm}}, E_t + \Phi_p)$ is the undisturbed intensity beyond the solar wind termination located at a radial distance r_{tm} from the Sun; E_t is the total energy of the particle with rest mass m_r and, finally, Φ_p is the so-called force-field energy loss (Gleeson & Axford 1968; Gleeson & Urch 1971). When modulation is small [i.e., for $\Phi_p \ll m_r c^2, T$] (Gleeson & Axford 1968; Gleeson & Urch 1971, 1973), they determined that

$$\Phi_p = \frac{ZeP}{K_P(P, t)} \phi_s(r, t) \approx Ze \phi_s(r, t),$$

where Ze is the particle charge and $\phi_s(r, t)$ is the so-called *modulation strength* (or *modulation parameter*) usually expressed in units of GV (or MV). Assuming that V_{sw} (the solar wind speed) and k_1 are almost constant, $\phi_s(r, t)$ is linearly dependent on $(r_{\text{tm}} - r)$ (e.g., see Equation (4.64) of Leroy & Rancoita 2011), from which one gets that the diffusion parameter is given by

$$k_1(t) \approx \frac{V_{\text{sw}}(t) (r_{\text{tm}} - r)}{3\phi_s(r, t)}, \quad (11)$$

i.e., k_1 [similarly to $\phi_s(r, t)$] is linearly dependent on $(r_{\text{tm}} - r)$. As already mentioned, in the FFM the diffusion coefficient $\mathcal{K}(r, t)$ is a scalar quantity and does not account for effects related to the charge sign of the transported particles. $\phi_s(r, t)$ is independent of the species of GCR particles (e.g., see discussion at page 1014 of Gleeson & Axford 1968 or Equation (1) of Usoskin and collaborators 2005, and also Bobik et al. 2011a,b). Usoskin and collaborators 2005 monthly determined the values of the modulation strengths [$\phi_s(r_{\text{Earth}})$] for the time

⁴While in Eq. (1), it is expressed by a tensor with a symmetric and an antisymmetric part (see discussion in Sect. 2).

period from 1951 up to 2004 using measurements of neutron monitors (i.e., located at $r_{\text{Earth}} = 1 \text{ AU}$); while the values of solar wind speeds are available from NASA/GSFC’s OMNI data set through OMNIWeb.

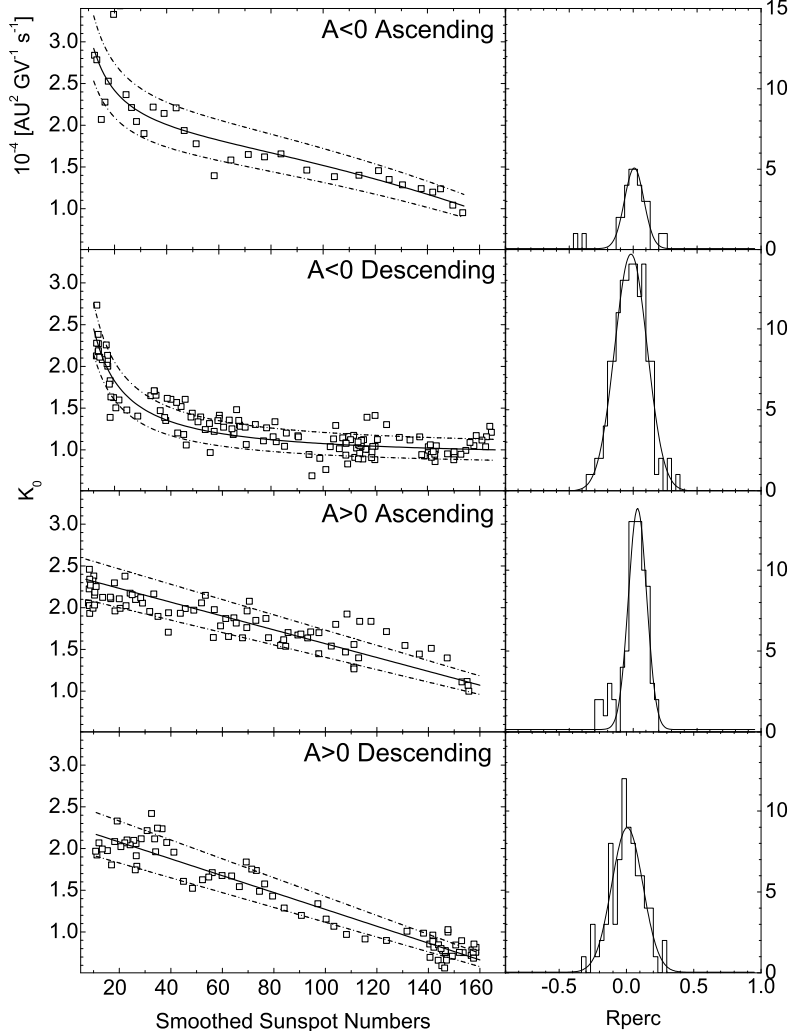


Fig. 1.— Diffusion parameter K_0 (left side) and percentage differences R_{perc} [Eq. (14)] (right side) as a function of the SSN value; the central continuous lines are obtained from a fit of K_0 with respect to SSN values in the range $10 \lesssim \text{SSN} \lesssim 165$; the dashed and dotted lines are obtained adding (top) or subtracting (bottom) one standard deviation from the fitted values.

To determine $\phi_s(r_{\text{Earth}})$, Usoskin and collaborators (2005) used an approximated expression of the Local Interstellar Spectrum (LIS) for protons from Burger, Potgieter and Heber (2000). In practice, their spectrum differs from that due to Burger, Potgieter and

Solar polarity and phase	$A < 0$ ascending	$A < 0$ descending	$A > 0$ ascending	$A > 0$ descending
c_1	+0.0001686	$+8.872 \times 10^{-5}$	$+2.39708 \times 10^{-4}$	$+2.28037 \times 10^{-4}$
c_2	+0.001488	+0.001874		
c_3			-8.28987×10^{-7}	-1.00984×10^{-6}
c_4	-3.164×10^{-9}			

Table 1: Parameters of the polynomial expression (13).

Heber (2000) by about or more than 5% at kinetic energies lower than about 117 MeV. Furthermore, in the present work we found that the error-weighted average of the differential spectral index, γ_{wa} [Eq.(31) and discussion in Sect. 7.1], of the proton LIS is only compatible, within one standard deviation, with the differential spectral index ($\gamma = 2.78$) of the spectrum from Burger and Potgieter (1989) or Burger, Potgieter and Heber (2000). It has to be remarked that the latter spectral index is the one used by Usoskin and collaborators (2005). Usoskin and collaborators (2005) [see Appendix A in that article] also found that using other commonly adopted LIS's their corresponding values of the modulation strengths follow a linear relation with respect to $\phi_s(r_{\text{Earth}})$. However, the differential spectral indexes of these spectra are not compatible within three or more standard deviations with that found in Sect. 7.1. Moreover, it has to be noted that the response of neutron monitors has to be evaluated by combining a) the effects of both the geomagnetic cutoff rigidity (Usoskin et al. 2005) which results in a reduced sensitivity of detection apparatus and b) the so-called *atmospheric yield function* (Clem & Dorman 2000). Thus, one finds that i) the contribution of the GCRs with rigidities below 2 GV amounts to about or less than 1.1% of the total neutron monitor counts due to particles with energies up to about 50 GV and ii) the maximum of neutron monitor sensitivity - i.e., the maximum of the response function [see Figure 7 of Clem & Dorman (2000)] - occurs in the rigidity interval (3–15) GV. In addition, Boella and collaborators (2001) determined - using IMP8 satellite data during the period 1973–1995 - that charge effects (discussed in Sects. 1, 2) result in a variation of proton or helium fluxes during solar minima with opposite magnetic field polarities of $14 \pm 6\%$ at ≈ 300 MeV/nucleon. This variation steadily decreases with increasing energy [e.g., see Figure 4.13 at page 378 of Leroy & Rancoita (2011)]. As a consequence, $\phi_s(r_{\text{Earth}})$ is expected to be marginally affected by drift effects.

k_1 [Eq. (11)] depends on the value of solar wind termination located at a radial distance r_{tm} related, in turn, also to solar wind speed [e.g., see Chapter 7 of Meyer-Vernet (2007),

and Sections 4.1.2.3, 4.1.2.4 of Leroy & Rancoita (2011)]. In the present simulation code, the *effective heliosphere* assumes that the solar wind termination is located at 100 AU (see a further discussion in Sects. 5, 7.3). Therefore, from the diffusion parameter k_1 one has to derive that (K_0) for an effective heliosphere with a radial extension of 100 AU. In practice, for a radial extension of 100 AU the diffusion parameter K_0 [Eq. (12) replaces k_1 in Eq. (6) (for instance, see Appendix A) and in allows one to obtain similar modulation effects on the differential intensities of GCRs with respect to those obtained using k_1 when the heliosphere has a variable radial extension r_{tm} . Using Eq. (11) one obtains

$$K_0 \approx k_1 \frac{99 \text{ AU}}{(r_{\text{tm}} - r_{\text{Earth}})} = 99 \text{ AU} \left[\frac{V_{\text{sw}}}{3 \phi_{\text{s}}(r_{\text{Earth}})} \right], \quad (12)$$

where 99 AU (as already mentioned) is the distance of the Earth from the border of the effective heliosphere used in the current simulation code. In Fig. 1, the diffusion parameter K_0 - obtained from Eq. (12) - is shown as a function of the corresponding value of smoothed sunspot number, SSN, (SSN 2010). The K_0 data had to be subdivided in four sets, i.e., ascending and descending phases for both negative and positive solar magnetic-field polarities. For each set, the data could be fitted with a *practical relationship* (see Fig. 1) between K_0 and SSN values for $10 \lesssim \text{SSN} \lesssim 165$, i.e., finding

$$K_{\text{F}} = c_1 + c_2 \times \text{SSN}^{-1} + c_3 \times \text{SSN} + c_4 \times \text{SSN}^2 \quad (13)$$

with the parameters c_i shown in Table 1. In addition, the data were found to exhibit a Gaussian distribution of percentage differences (R_{perc}) of K_0 values from the corresponding fitted values K_{F} , with

$$R_{\text{perc}} = \frac{K_{\text{F}} - K_0}{K_{\text{F}}}. \quad (14)$$

The rms values of the Gaussian distributions were found to be $\approx 0.1339, 0.1254, 0.1040, 0.1213$ for the phases ascending with $A < 0$, descending with $A < 0$, ascending with $A > 0$, descending with $A > 0$, respectively. From the practical relationship found [Eq. (13)], we can use the estimated SSN values to obtain the diffusion parameter K_0 at times beyond 2004. This procedure allows one to extend the ≈ 40 years period by exploiting the practical relationship between the fitted K_0 values and the SSN values (one of the main parameters related to the solar activity). In addition, we introduced in our code a Gaussian random variation of K_0 with rms's corresponding to those found for each subset of data. Results of the simulation with and without the Gaussian variation are consistent within the uncertainties of the code. Furthermore, it can be noted that K_0 results in providing an overall increasing (for r_{tm} lower than 100 AU) or decreasing (for r_{tm} larger than 100 AU) of modulation effects. A tuning of the effective extension of the heliosphere and its dependence on the solar activity is likely to be obtained using the experimental data from long-duration accurate observations, like those from the AMS-02 spectrometer.

3. Solar Wind and Latitudinal Dependence IMF

Parker (1958) suggested that the solar corona is stationary expanding due to an outflow of the coronal plasma - generating the so-called *solar wind* - with a spherically symmetric velocity. In his model, the solar wind speed becomes almost constant (V_{sw}) beyond a radial distance from the Sun $r_b \approx (0.3\text{--}0.4)$ AU (e.g., see Figure 1 of Parker 1958). Furthermore, the magnetic-field lines are frozen in the streaming particles of which the solar wind consists. Thus, beyond r_b , in a spherical reference frame rotating with the Sun the components of the outward velocity of a plasma element carrying the magnetic field are: $V_r = V_{\text{sw}}$, $V_\theta = 0$ and $V_\phi = \omega(r - r_b) \sin \theta$ with ω the angular velocity of the Sun. The streamline has the shape of an Archimedean spiral (termed *Parker spiral*).

In heliocentric spherical coordinates, the standard Parker spiral field can be expressed as (e.g., see Equation (2) of Hattingh & Burger 1995):

$$\vec{B}_P = \frac{A}{r^2} (\vec{e}_r - \Gamma \vec{e}_\phi) [1 - 2H(\theta - \theta')], \quad (15)$$

where A is a coefficient that determines the field polarity and allows $|\vec{B}_P|$ to be equal to B_\oplus (Sect. 2), i.e., the value of IMF at Earth's orbit as extracted from NASA/GSFC's OMNI data set through OMNIWeb (King & Papatashili 2005); \vec{e}_r and \vec{e}_ϕ are unit vector components in the radial and azimuthal direction, respectively; θ is the co-latitude (polar angle); θ' is the polar angle determining the position of the HCS (Jokipii & Thomas 1981); H is the Heaviside function, thus, $[1 - 2H(\theta - \theta')]$ allows \vec{B}_P to interchange the sign in the two regions - above and below the heliospheric current sheet (HCS) - of the heliosphere; finally,

$$\Gamma = \tan \psi = \frac{\omega (r - r_b) \sin \theta}{V_{\text{sw}}} \quad (16)$$

with ψ the spiral angle. In the present, model ω is assumed to be independent of the heliographic latitude and equal to the *sidereal rotation* at the Sun equator. However, the simple representation of the Parker spiral [Eqs. (15, 16)] based on a constant solar wind speed needs to be complemented with the present knowledge of the speed $[V_{\text{sw}}(\theta)]$ dependence on solar colatitude. Large variations of the solar wind structure were observed for solar latitudes up to $|80^\circ|$ by Ulysses spacecraft (Wenzel et al. 1992). For instance, during a period of low solar activity the solar wind speed increases by almost a factor two from the ecliptic plane to poles, thus subdividing the heliosphere in two regions with slow and fast solar wind (Mc Comas et al. 2000). For representing the observed speeds, Fichtner, Ranga and Fahr (1996) suggested that the solar wind speed may be proportional to $(1 + \cos^2 \theta)$. In the present model we use:

$$V_{\text{sw}}(\theta) = \begin{cases} V_{\text{sw}_{\text{max}}}, & \text{for } \theta \leq 30^\circ \text{ and } \theta \geq 150^\circ, \\ V_{\text{sw}_{\text{min}}} \times (1 + |\cos \theta|), & \text{for } 30^\circ < \theta < 150^\circ \end{cases} \quad (17)$$

with $V_{sw_{max}} \simeq 760$ km/s (e.g., see Mc Comas et al. 2000)] and $V_{sw_{min}}$ is the corresponding value extracted from NASA/GSFC’s OMNI data set through OMNIWeb (King & Papatashili 2005). Equation (17) exhibits a slightly better agreement with observed data than that proposed by Fichtner, Ranga and Fahr (1996). Jokipii and Kóta (1995) and Pommois, Zimbardo and Veltri (2001) proposed other functions for such periods. However, these functions depends on an additional parameter related to the latitudinal extension of the region with a slow solar wind. The parameter can be determined only using measurements to be performed largely outside the ecliptic plane, like those due to Ulysses spacecraft. Thus, Eq. (17) has the advantage to allows one to more generally treat periods of low solar activity. Furthermore, McComas and collaborators (2000) observed that during the Sun’s approach to solar maximum a) the coronal structure becomes increasingly complex and b) the magnetic field becomes less dipolar. In the present model, for the solar wind we assume a speed independent of the colatitude in periods characterized by a large solar activity. As previously, the speed value is extracted from NASA/GSFC’s OMNI data set through OMNIWeb (King & Papatashili 2005).

Potgieter et al. (1989) pointed out how *classical drift* modulation models - based on the Parker magnetic-field up to the polar region - encounter difficulties (see also Sect. 7.4) in accounting for the significantly lower latitudinal dependence of CRs intensity. Simpson (1996) subsequently observed this phenomenon using Ulysses spacecraft data collected in the inner heliosphere. Heber and collaborators (1998) remarked that a) one needs to assume an anisotropy of perpendicular diffusion coefficient and enhancement in the latitude direction (as already treated in Sect. 2), and b) Parker’s IMF has to be modified⁵ as proposed by Jokipii and Kóta (1989).

In the present model, the magnitude of the magnetic field [Eq. (15)] is enhanced introducing a small latitudinal component (e.g., see Langner 2004; Langner & Potgieter 2004)

$$B_{\theta} = \frac{A}{rr_{\odot}}\delta(\theta) \quad (18)$$

with r_{\odot} the solar radius,

$$\delta(\theta) = \frac{8.7 \times 10^{-5}}{\sin \theta}; \quad (19)$$

for $\theta \lesssim 1.7^{\circ}$ and $\theta \gtrsim 178.3^{\circ}$, δ is $\simeq 3 \times 10^{-3}$ (Fichtner et al. 1996). It has to be noted that Eqs. (18, 19) allows one to obtain $\nabla \cdot \vec{B} = 0$. The magnitude of the magnetic field used in

⁵Limited to polar regions, Fisk (1996) proposed that magnetic-field lines are non radially expanding. In addition, Hitge and Burger (2010) have attempted to merge Parker and Fisk magnetic-fields into a hybrid field.

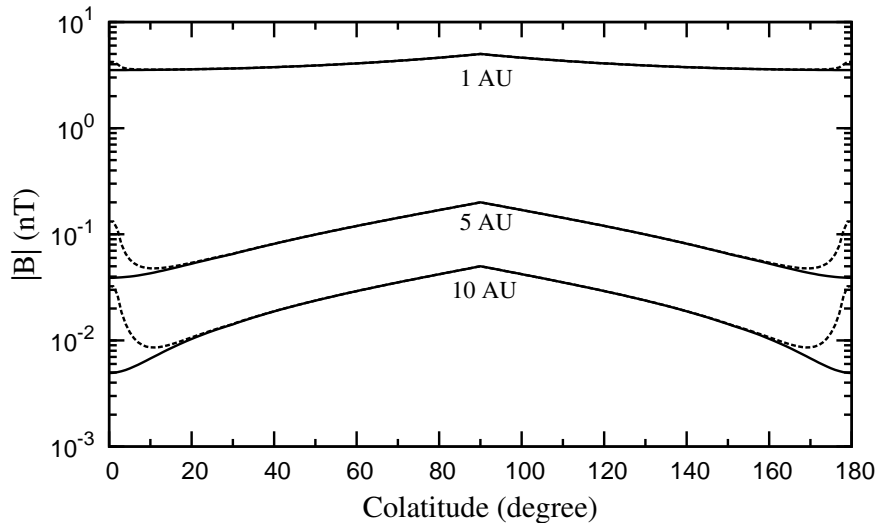


Fig. 2.— Magnitude ($|B|$) of the IMF (dashed line) from (Kóta & Jokipii 1989) - computed using Eqs. (18–20) - compared with that from Parker (solid line) [Eq. (15)] at 1, 5 and 10 AU as a function of the colatitude. For the purpose of this calculation, at 1 AU and 90° $|B| = 5$ nT.

the current model is given by (Jokipii & Kóta 1989):

$$B = \frac{A}{r^2} \sqrt{1 + \Gamma^2 + \left(\frac{r}{r_\odot}\right)^2 \delta^2(\theta)}. \quad (20)$$

In Fig. 2, the magnitude ($|B|$) of the IMF from (Kóta & Jokipii 1989) is compared with that from Parker [Eq. (15)] at 1, 5 and 10 AU as a function of the colatitude: the field magnitude significantly increases in the polar regions (colatitude $\lesssim 10^\circ$ and $\gtrsim 170^\circ$), while it is almost unchanged in the ecliptic region (colatitude $\approx 90^\circ$). $|B|$ (Fig. 2) was computed using Eqs. (18–20). As discussed by Haasbroek and Potgieter (1995), the above modification of the Parker IMF allows the modulation effect in the polar regions to be increased and, subsequently, more realistic radial and latitudinal gradients.

As well known (e.g., see Bravo et al. 1998, and references therein), during several years around solar minimum the general structure of the solar magnetic-field is more or less axially symmetric, dominated by the dipole component. These periods are characterized with corresponding low values of the tilt angle ($\alpha_t < 30^\circ$, Potgieter et al. 2001). As the solar activity increases, the dipolar structure inclines more and more with respect to the rotation axis and the effect of higher multipoles becomes more relevant (Sanderson et al. 2003). During the years of high activity, the structure of the solar magnetosphere is very complex

and the dipole component is very tilted (e.g., see Sanderson et al. 2003; Wang & Sheeley 2002). These periods are characterized with corresponding large values of the tilt angle ($\alpha_t > 75^\circ$, Potgieter et al. 2001). Finally, one can remark that, dealing with neutron-monitor measurements, Cliver & Ling (2001) concluded that a diffusion/convection dominated modulation occurs when the tilt angle exceeds 50° [for a previous discussion and illustration with numerical models, e.g., see Potgieter (1995) and references therein].

In the current model the evolution of the solar magnetosphere and, subsequently, of the IMF is (partially) taken into account using the diffusion parameter (treated in Sect. 2.1) and the actual value of tilt angle. In fact, the diffusion parameter depends on the solar phase (ascending and descending) and solar polarity (positive and negative), and is practically related to the actual value of smoothed sunspot number via Eq. (13); while the tilt angle allows one to gradually modify the contribution of drift effects to modulation (Sect. 4). The agreement with data obtained during high (low) solar activity is discussed in Sect. 7.2 (Sect. 7.2.1).

4. The Neutral Sheet and Large Scale Gradients of IMF

K_A expresses the value of the *antisymmetric part of the diffusion tensor* and results from the effects on the motion of cosmic-ray particles due to drift mechanisms. In a coordinate system with the 3rd coordinate along the average IMF, one finds (e.g., see Potgieter & Moraal 1985; Burger & Hattingh 1995)

$$K_A = \frac{pv}{3Ze|B|}, \quad (21)$$

where p , v and Ze are the momentum, velocity and charge of the cosmic-ray particle, respectively. Thus, the antisymmetric elements of the diffusion-tensor matrix (Sect. 2) are

$$K_{ij}^A = K_A \epsilon_{i,j,k} \frac{B_k}{|B|}$$

with $\epsilon_{i,j,k}$ the *Levi-Civita symbol* (e.g., see Equation (10) of Parker 1965).

As already mentioned in Sect. 2, the *drift velocity* \vec{v}_d [Eq. (2)] accounts i) for effects due to gradient and curvature drifts experienced by cosmic-rays particles transported through the IMF, ii) net drift effects occurring close to the HCS, where the IMF changes polarity (e.g., see Parker 1957; Burger, Moraal & Webb 1985; Potgieter & Moraal 1985) and iii) can be calculated using the antisymmetric part of the diffusion tensor (e.g., see Parker 1965; Jokipii et al. 1977; Potgieter & Moraal 1985; Burger & Hattingh 1995, and references therein).

Burger, Potgieter and Heber (2000) [see also references therein and (Palmer 1982; Lockwood & Webber 2000)] remarked that the observational results (carried out below 5 GV)

are consistent with a small (or very small) ratio of the perpendicular to parallel diffusion coefficients. As discussed by Parker (1965), a small value of that ratio indicates that cosmic-rays particles are practically moving through several gyro-orbits between each scattering event, i.e., drift motion is *weakly affected by scattering*. In addition, for cosmic-rays particles with rigidities $\lesssim (10\text{--}15)$ GV and an IMF expressed by Eqs. (15, 20), the particle gyro-radius is smaller (or much smaller) than any local (i.e., inside the heliosphere) scale variation of magnetic field $L \equiv |(1/B)(\partial B_i/\partial x_i)|^{-1}$. In this way, for regions outside that of HCS, Isenberg and Jokipii (1979) remarked that \vec{v}_d is determined by the terms due to the gradient and curvature drifts (e.g., see also Parker 1957; Armstrong et al. 1985).

Potgieter and Moraal (1985) treated the modulation of GCR's for steady state conditions with relevant drift effects including that due to a wavy HCS (WHCS). They succeeded in formulating a 2-D description (of the WHCS), which - as discussed by Burger and Hattingh (1995) - is equivalent to the treatment of transport in a three-dimensional heliosphere with the assumption of an axis-symmetric particle distribution. Thus, they allowed one to neglect the azimuthal dependence. The effect of a WHCS was included via an appropriate modification of the antisymmetric part of the diffusion tensor. In this 2-D modeling, the WHCS is described as a wide region whose width depends on the rigidity of cosmic-ray particles and actual value of the tilt angle (α_t). The resulting drift velocity in heliocentric polar coordinates - as used in the current model - is given by (e.g., see Equation (6) of Burger & Hattingh 1995):

$$\vec{v}_d = f(\theta)\nabla \times \left(K_A \frac{\vec{B}}{B} \right) + \left(\frac{\partial f(\theta)}{\partial \theta} \right) \frac{K_A}{r} \vec{e}_\theta \times \left(\frac{\vec{B}}{B} \right) \quad (22)$$

$$= \vec{v}_{\text{dr}} + \vec{v}_{\text{HCS}}, \quad (23)$$

where K_A is from Eq. (21), θ is the colatitude, $f(\theta)$ is a *transition function* that accounts for the effects of a wavy neutral sheet (Potgieter & Moraal 1985) and \vec{e}_θ is the unit vector along the latitudinal direction. $f(\theta)$ is expressed as (e.g., see Equation (14) of Potgieter & Moraal 1985):

$$f(\theta) = \begin{cases} (1/a_h) \arctan \{ \{1 - [(2\theta)/\pi]\} \tan(a_h) \}, & \text{if } c_h < \frac{\pi}{2}, \\ 1 - 2H[\theta - (\pi/2)], & \text{if } c_h = \frac{\pi}{2} \end{cases}$$

with H the Heaviside function,

$$a_h = \arccos \left(\frac{\pi}{2c_h} - 1 \right)$$

(e.g., see Equation (15) of Potgieter & Moraal 1985),

$$c_h = \frac{\pi}{2} - \frac{1}{2} \sin(\alpha_t + \Delta\theta_{\text{HCS}})$$

(e.g., see Equation (23) of Burger & Potgieter 1989),

$$\Delta\theta_{\text{HCS}} = \frac{2r_p}{r}$$

(r_p is the particle gyro-radius, e.g., see Hattingh & Burger 1995 and also Section 4.2 of Burger & Hattingh 1995), finally, $f(c_h) = 0.5$ and $f(\pi/2) = 0$. $\Delta\theta_{\text{HCS}}$ is determined from the maximum distance that a particle drifting along the neutral sheet can be away from this sheet (Burger & Potgieter 1989). The first term (\vec{v}_{dr}) of Eq. (22) accounts for the gradient and curvature drifts, the second (\vec{v}_{HCS}) for drift in the region affected by a WHCS. The transition function sets the rate at which the first term of Eq. (22) goes to 0 on the ecliptic plane ($\theta = \pi/2$) (Potgieter & Moraal 1985).

5. Parameters of the Effective Heliosphere used in the Current Model

As discussed by Potgieter (2008) (see also references therein), until recently the heliosphere was assumed to be spherical in most modulation models with an outer boundary at radial distances beyond ≈ 100 AU. Presently, the heliospheric structure is considered latitudinally asymmetric (particularly) during solar minimum conditions mostly because the SW depends on the latitude and solar activity (Sect. 3). As a consequence, the position of termination shock (where the SW ram pressure is balanced by interstellar pressure), TS, can exhibit a latitudinal asymmetry.

Using solar wind speeds observed from Ulysses, Whang and collaborators (e.g., see Whang & Burlaga 2000; Whang et al. 2003, 2004) could estimate the radial position of TS on and outside the ecliptic plane. They found that a) on the ecliptic the radial distance of TS is about of 80 AU on average (without large variation between low and high solar activities), b) near the ecliptic the radial distance varies by less then 20 AU and c) outside the ecliptic plane (e.g., at a latitude of 35°) the location of the TS increases by more than or about 50 AU (Whang et al. 2003). In addition, Whang and collaborators estimated that the averaged value over a 26-years period of the radial distance of the TS increases with latitude [see Table 2 of (Whang et al. 2003)]. It is worthwhile to remark that ≈ 100 AU is the averaged value over the corresponding solid angle of the TS location, which can be obtained from Table 2 of (Whang et al. 2003). Furthermore (e.g., see Stone et al. 2005, 2008), Voyager 1 and 2 reached the TS in 2004 and 2007 located at about 94.0 AU and 83.7 AU, respectively, in agreement with the predictions from Whang and collaborators. Langner and Potgieter (2005) treated symmetric and asymmetric TS models and concluded that for $A > 0$ cycle for solar minimum no significant difference occurs; for $A < 0$ cycle differences remain insignificant in nose direction while, approaching the tail direction, some differences can be

appreciated at proton energies below (1–1.5) GeV. However, Langner and Potgieter (2005) and Potgieter (2008) suggested that, in general, a symmetric TS with a radial distance of ≈ 100 AU is still a reasonable assumption.

In the present model (as already discussed in Sect. 2.1), the effect of the modulation is obtained for the GCRs propagation through a symmetric effective heliosphere with a radius of 100 AU. The diffusion parameter K_0 is determined (following the procedure described in Sect. 2.1) using the values of modulation strength, SSN values (SSN 2010) and radius of the effective heliosphere. Furthermore, it has to be remarked that (see discussion in Sect. 2.1) the atmospheric yield function results in a diffusion parameter related to modulated intensities of GCRs (mostly protons) with rigidities above 2 GV.

Other parameters (which depend on the solar activity) are the tilt angle α_t of the HCS, magnetic field polarity [related to the sign of the coefficient A in Eq. (15)], magnetic field magnitude (B_\oplus) and solar wind velocity (V_{sw}). The latter two parameters are measured at Earth’s orbit. The polarity of the magnetic field and B_\oplus determines the IMF described by means of Eqs. (15, 16, 18–20). α_t and the field polarity are used to deal with the drift velocity (as discussed in Sect. 4), which modifies the overall convection velocity [Eq. (4)]. Drift contribution is relevant during low solar activity - e.g., for $\alpha_t < 30^\circ$ (Sect. 3) - and decreases with increasing solar activity. α_t values are obtained from Wilcox Solar Observatory (Hoeksema 1995; WSO 2010) and are calculated using two different models called “R” and “L”. Ferreira & Potgieter (2003, 2004) suggested that “R” model accounts for GCR observations during periods of increasing solar activity (for instance, 1987.4–1990.0 and 1995.5–2000.0), while “L” model accounts for periods of decreasing solar activity (for instance, 1990.0–1995.5 and 2000.0–2010.0). The implementation of “R” and “L” models in the current code is further treated in Sects. 7.2–7.2.1. Finally, the latitudinal dependence (e.g., see Sect. 3) of the solar wind [Eq. (17)] depends (at low solar activity) on the values (averaged over 27 days) of SW speed and on the ecliptic at Earth orbit.

The time spent by the SW to cover the distance from the outer corona up to the boundary of the effective heliosphere can be expressed in units of the time needed for a sidereal rotation on the equator of the Sun (about 25 days, e.g., see page 77 of Aschwanden 2006 and also Brajša et al. 2001; for a survey see Ruždjak et al. 2005). For instance depending on the wind speed, on the ecliptic the SW spends the corresponding amount of time needed to complete from 12 up to 20 sidereal solar rotations to reach the outer boundary. In the present code, the effective heliosphere (with a radius of 100 AU) was subdivided in 15 spherical regions. In each region, the parameters (e.g., SW speed, K_0 , B_\oplus , α_t , etc.) are determined at the time of the solar wind ejection.

6. The Monte Carlo Code HelMod

It is worthwhile to note that Eqs. (1, 4) can be analytically solved only treating a simplified transport of GCRs through the heliosphere (e.g., see Sect. 2.1 and also Gleeson & Axford 1968; Caballero-Lopez & Moraal 2004). Complex configurations regarding the transport inside the heliosphere were proposed using numerical methods, like finite-difference integration (e.g., Burger & Potgieter 1989).

As implemented in the HelMod code⁶ version 1.5, the current approach i) follows that from Yamada et al. (1998); Gervasi et al. (1999); Zhang (1999); Alanko et al. (2003); Pei et al. (2010b); Strauss et al. (2011) and ii) exploits a Monte Carlo technique to determine the number density U (Sect. 2) using the set of the approximated stochastic differential equations (SDEs) treated in Appendix A for a 2-D approximation (radial distance and colatitude). For a) an IMF described by the standard Parker field [Eq. (15)] and b) both solar wind and drift velocity in the region of WHCS radially directed (e.g., $V_{\text{sw},r} = V_{\text{sw}}$ and $v_{\text{HCS},r} = v_{\text{HCS}}$), the SDEs approximated in terms of the increments Δr , $\Delta\mu(\theta)$, ΔT and Δt [with $\mu(\theta) \equiv \cos(\theta)$] are (see Appendix A):

$$\Delta r = \frac{1}{r^2} \left[\frac{\partial}{\partial r} (r^2 K_{rr}^S) \right] \Delta t + (V_{\text{sw}} + v_{\text{dr},r} + v_{\text{HCS}}) \Delta t + \omega_r \sqrt{2K_{rr}^S \Delta t}, \quad (24)$$

$$\begin{aligned} \Delta\mu(\theta) = & \frac{1}{r^2} \left\{ \frac{\partial}{\partial\mu(\theta)} \{ [1 - \mu^2(\theta)] K_{\theta\theta}^S \} \right\} \Delta t - \frac{v_{\text{dr},\theta} \sqrt{1 - \mu^2(\theta)}}{r} \Delta t \\ & + \omega_{\mu(\theta)} \sqrt{\frac{2 K_{\theta\theta}^S [1 - \mu^2(\theta)]}{r^2}} \Delta t, \end{aligned} \quad (25)$$

$$\Delta T = -\frac{2}{3} \frac{\alpha_{\text{rel}} V_{\text{sw}} T}{r} \Delta t \quad (26)$$

[see Equations (2–4) of Bobik et al. 2011d, see also Pei et al. 2010b and references therein]. For the IMF treated in Sect. 3 [Eqs. (18–20)] the SDEs [Eqs. (A25–A27)] can be approximated with [Eqs. (A31–A33)]:

$$\begin{aligned} \Delta r = & \left\{ \frac{1}{r^2} \frac{\partial}{\partial r} (r^2 K_{rr}^S) - \frac{\partial}{\partial\mu(\theta)} \left[\frac{K_{r\theta}^S \sqrt{1 - \mu^2(\theta)}}{r} \right] + V_{\text{sw}} + v_{\text{dr},r} + v_{\text{HCS}} \right\} \Delta t \\ & + \omega_r \sqrt{\frac{K_{rr}^S K_{\theta\theta}^S - (K_{r\theta}^S)^2}{0.5 K_{\theta\theta}^S}} \Delta t - \omega_{\mu(\theta)} K_{r\theta}^S \sqrt{\frac{2}{K_{\theta\theta}^S}} \Delta t, \end{aligned} \quad (27)$$

⁶In the 2D-HelMod code version 1.0, the standard Parker field without drifts was implemented; in version 1.2, the dependence on the particle drift was added; finally, in version 1.4, the Parker magnetic field was modified in polar zones.

$$\Delta\mu(\theta) = \left\{ \frac{1}{r^2} \frac{\partial}{\partial r} \left(r K_{\theta r}^S \sqrt{1-\mu^2(\theta)} \right) + \frac{\partial}{\partial \mu(\theta)} \left\{ \frac{K_{\theta\theta}^S [1-\mu^2(\theta)]}{r^2} \right\} - \frac{v_{\text{dr},\theta} \sqrt{1-\mu^2(\theta)}}{r} \right\} \Delta t + \omega_{\mu(\theta)} \sqrt{\frac{2K_{\theta\theta}^S [1-\mu^2(\theta)]}{r^2}} \Delta t, \quad (28)$$

$$\Delta T = -\frac{2}{3} \frac{\alpha_{\text{rel}} V_{\text{sw}} T}{r} \Delta t. \quad (29)$$

As discussed by Pei et al. (2010b) [see also (Strauss et al. 2011)], the vector $\vec{q} = (r, \mu, T)$ represents a so-called *pseudoparticle* (see Appendix A). Equations (27–29) allow one to simulate the time evolution of pseudoparticles from the outer boundary down to the inner heliosphere. As treated by Achterberg and Krulls (1992), the number density U - or equivalently the differential intensity J [Eq. (3)] - can be obtained from *the density of pseudoparticles* by averaging over many realizations of the SDEs.

The procedure to integrate the SDEs is the following: 1) events are isotropically generated on the outer border of the effective heliosphere; 2) each event is integrated over the time evolution of a pseudoparticle and is processed forward-in-time until it reaches either the outer (inner) border of the effective heliosphere located at 100 AU (r_b) or the pseudoparticle energy becomes lower than a minimum threshold (which depends on the set of experimental data taken into consideration), then a new particle is generated; 3) when a pseudoparticle reaches a particular region (for instance that corresponding to Earth position) its injection energy, statistical-weight, etc. are recorded; 4) finally, the number density U results from the normalized distribution function obtained using a procedure from Pei et al. (2010b) (see Section 4.3 in this article). The forward-in-time approach allows one to reproduce rigorously processes occurring inside the heliosphere.

In the present code, Δt varies as r^2/K_{rr} , thus allowing an increase of the accuracy in the inner heliosphere, but keeping the appropriate precision up to regions close to the outer border of the effective heliosphere. Furthermore, this condition ensures that the diffusion process is dominant (see Section 4.1 of Krulls & Achterberg 1994).

7. Results

The current modulation code (Sect. 6) provides a modulated differential intensity for protons using a local interstellar spectrum (LIS) of protons. In the following, we will discuss i) the LIS used (Sect. 7.1), ii) the comparison of simulated (modulated) differential intensities with those obtained from the measurements of BESS, AMS and PAMELA spectrometers during the solar cycle 23 (Sects. 7.2, 7.2.1) and iii) the dependence of present results on the

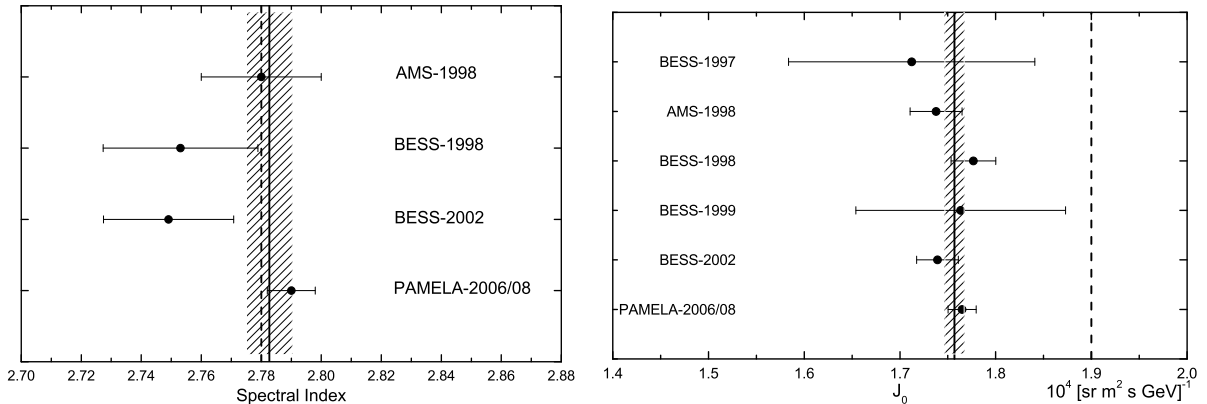


Fig. 3.— Left: spectral index (γ) obtained (see text) for AMS–1998, BESS–1998, BESS–2002 and PAMELA–2006/08. Right: normalization constant (J_0) for BESS–1997, AMS–1998, BESS–1998, BESS–1999, BESS–2002 and PAMELA–2006/08. The dotted lines represent the values of the spectral index (γ_{BPH}) and normalization constant ($J_{0,\text{BPH}}$) of the BPH-LIS, respectively; the continuous lines represent the error-weighted averages of spectral index (γ_{wa}) and normalization constant ($J_{0,\text{wa}}$).

treatment of the heliosphere extension (Sect. 7.3). Furthermore (Sect. 7.4), the simulated fluxes obtained with HelMod code are compared with (and found to reproduce the features of) the experimental data from Ulysses fast scan in 1995 (Simpson, Zhang and Bame 1996).

7.1. Local Interstellar Spectrum

Recently, Herbst et al. (2010) reviewed different proton LIS’s published in the literature and determined that - as it can be seen in Figure 2(b) in that article - these spectra agree well with each other for proton energies above 10 GeV. For this comparison, they used, among others, the LIS from Burger, Potgieter and Heber (2000) (BPH-LIS) in the form of the approximated analytical expression from Usoskin and collaborators (2005). Over the past years, Moskalenko, Strong and collaborators using GALPROP provided a LIS for protons [e.g., see Moskalenko et al. (2002); Strong & Moskalenko (2004); Trotta et al. (2011), see also Langner (2004); Langner et al. (2003)]: the latest calculation agrees with the BPH-LIS above 1 GV [e.g., see Trotta et al. (2011)]. It has to be remarked that the GALPROP spectrum is constrained by a few measured quantities (for instance, the B/C and other isotopes and/or nuclei ratios), some of them will be (accurately) re-determined in the coming years using data from PAMELA and AMS-02 missions.

In units of $(\text{sr m}^2 \text{s GeV})^{-1}$ (Burger et al. 2000, see also Usoskin et al. 2002) the BPH-LIS is expressed as:

$$J_{\text{BHP}}(T) = \begin{cases} J_{0,\text{BHP}} R^{-\gamma_{\text{BPH}}}, & \text{for } R \geq 7, \\ \exp[9.472 - 1.999 \ln R - 0.6938 (\ln R)^2 \\ + 0.2988 (\ln R)^3 - 0.04714 (\ln R)^4], & \text{for } R < 7, \end{cases} \quad (30)$$

with

$$R \equiv R(T) = \frac{P(T)}{P_0},$$

where

$$P(T) = \frac{\sqrt{T(T + 2E_{r,p})}}{e}$$

(e.g., see Equation (4.94) in Leroy & Rancoita 2011) is the proton rigidity in GV with $E_{r,p} = m_p c^2$, m_p is the rest mass of protons in GeV/c^2 , T is the kinetic energy of proton in GeV, e is the electron charge, c is the speed of light, $\gamma_{\text{BPH}} = 2.78$ is the spectral index, $J_{0,\text{BHP}} = 1.9 \times 10^4 (\text{sr m}^2 \text{s GeV})^{-1}$ is a normalization constant and, finally, $P_0 = 1 \text{ GV}$.

Above (10–20) GeV the differential proton intensities are slightly or marginally affected by modulation. The BPH-LIS [first line of Eq. (30)] was compared to experimental spectra available in the literature and collected during the solar cycle 23. These observations also account for data in the energy range where modulation is relevant, e.g., AMS–1998 (Aguilar et al. 2002), BESS–1998 [with data only in the range (20–117) GeV] (Sanuki et al. 2000), BESS–2002 (Haino et al. 2004) and PAMELA–2006/08 (Adriani et al. 2011a). In Fig. 3, the spectral indexes (γ) of AMS–1998 and PAMELA–2006/08 are those from (Aguilar et al. 2002; Adriani et al. 2011b), respectively; while for BESS–1998 and BESS–2002 the spectral indexes were obtained from a fit to the published data of the differential proton intensities. It has to be noted that the rigidity independent part of the spectral index found by PAMELA–2006/08 is $\gamma_{\text{PAMELA}} = 2.790 \pm 0.008(\text{stat}) \pm 0.001(\text{syst})$; Adriani and collaborators (2011b) found that the spectral index depends on rigidity as expressed in Equation (19) therein with a maximum variation of the order of the previously quoted uncertainties in the rigidity range (30–200) GV. Furthermore, the spectral index (2.79 ± 0.08) found by Caprice–1994 (Boezio et al. 1999) is in agreement with those found by the experiments discussed in this section, but the quoted errors are larger.

The normalization constants J_0 (Fig. 3) a) depend on the set of experimental observations, e.g., BESS–1997 (Shikaze et al. 2007), BESS–1998 (Shikaze et al. 2007; Sanuki et al. 2000), AMS–1998 (Aguilar et al. 2002), BESS–1999 (Shikaze et al. 2007), BESS–2002 (Haino et al. 2004) and PAMELA–2006/08 (Adriani et al. 2011a) and b) were obtained from a fit using

γ_{BPH} as spectral index to the experimental data. For BESS–2000 (Shikaze et al. 2007), the experimental observations did not exceed the 21.5 GeV, i.e., an energy region of proton differential intensity which might (marginally) still be affected by modulation in a period of high solar activity; thus, the normalization constant used for these data was the one obtained from BESS–2002 (Haino et al. 2004) data.

The weighted averages of both the spectral index (γ) and normalization constant (J_0) and their errors were determined following the procedure indicated at pages 14–15 of PDB (2010). The error-weighted averages found are

$$\gamma_{\text{wa}} = 2.783 \pm 0.009 \quad (31)$$

and

$$J_{0,\text{wa}} = (1.76 \pm 0.01) \times 10^4 \text{ (sr m}^2 \text{ s GeV)}^{-1}. \quad (32)$$

γ_{wa} is well in agreement with that (γ_{BPH}) suggested by Burger, Potgieter and Heber (2000) [Eq. (30)]. $J_{0,\text{wa}}$ and γ_{wa} are represented with the continuous lines in Fig. 3; in the same figure the dotted lines refer to the values of the BPH-LIS [Eq. (30)]. It has to be remarked that the value of J_0 found from a fit to Caprice–1994 data above 20 GeV (Boezio et al. 1999) is 1.44 ± 0.02 : this value differs by more than 5 standard deviations from $J_{0,\text{wa}}$ [Eq. (32)].

In Sects. 7.2–7.2.1, using the current modulation code the observed proton spectra are compared with the modulated differential intensities obtained from an interstellar differential (per unit of kinetic energy) proton intensity [$J_{\text{HelMod}}(T)$] given by

$$J_{\text{HelMod}}(T) = J_{\text{BHP}}(T) \left(\frac{J_0}{J_{0,\text{BHP}}} \right) \text{ [sr m}^2 \text{ s GeV)}^{-1}. \quad (33)$$

$J_{\text{HelMod}}(T)$ keeps the same spectral index for $P(T) \geq 7 \text{ GV}$ as in Eq. (30) and linearly depends on J_0 , which accounts for the slight absolute fluxes variation among observations.

7.2. Comparison with Observations Obtained During Solar Cycle 23

We used the present code for quantitative comparisons [using Eqs. (34, 35)] with experimental data (discussed later in this section) collected during solar cycle 23, in periods with *high solar activity*, i.e., when the solar magnetic field becomes increasingly complex and less dipolar (Sects. 2, 3). This code allowed us to investigate how the modulated (simulated) differential intensities are affected by the i) particle drift effect (Sects. 2, 4), ii) polar enhancement of the diffusion tensor along the polar direction ($K_{\perp\theta}$) [Eq. (8)] and, finally, iii) the value of tilt angles (α_t) calculated following the approach due to “R” and “L” models

	“L” model	“R” model	<i>no drift</i>	<i>diagonal approx.</i>	<i>scalar approx.</i>
BESS–1999	8.7	8.0	14.6	32.0	29.7
BESS–2000	16.2	15.8	13.0	23.6	26.7
BESS–2002	12.7	15.0	12.2	34.8	33.2

Table 2: For BESS–1999, BESS–2000 and BESS–2002, η_{RMS} (in percentage) obtained from Eq. (34) *with enhancement of the diffusion tensor along the polar direction* using “L” and “R” models for the tilt angle and for *no drift* approximation, *diagonal approximation* and, finally, *scalar approximation* (see text).

	“L” model	“R” model	<i>no drift</i>	<i>diagonal approx.</i>	<i>scalar approx.</i>
BESS–1999	6.8	8.1	24.3	30.5	30.2
BESS–2000	11.3	10.2	10.8	26.2	26.2
BESS–2002	13.0	15.7	12.7	33.9	33.2

Table 3: For BESS–1999, BESS–2000 and BESS–2002, η_{RMS} (in percentage) obtained from Eq. (34) *without any enhancement of the diffusion tensor along the polar direction* using “L” and “R” models for the tilt angle and for *no drift* approximation, *diagonal approximation* and, finally, *scalar approximation* (see text).

[Sect. 5 and (Hoeksema 1995; WSO 2010)]. The magnetic field is modified with respect to Parker’s magnetic field in the polar region as proposed by Kóta & Jokipii (1989) (Sect. 3).

The effects related to particle drift were investigated (a) via the suppression of the drift velocity - i.e., under the assumption that $K_A = 0$ (Sect. 4), thus *no drift* convection was accounted for -, (b) in a pure diffusion approximation with a diagonal diffusion tensor (termed *diagonal approximation*), where $K_{rr} = \mathcal{K}$ and $K_{\theta\theta} = \rho_k \mathcal{K}$ (Sect. 2) and, finally, (c) in a pure diffusion approximation with components both equal to \mathcal{K} (called *scalar approximation*) [as in Eq. (9)]. The case (a) accounts the hypothesis that magnetic drift convection is almost completely suppressed during solar maxima. In addition, for cases (b) and (c) one allows to assume that the diffusion propagation is independent of magnetic structure.

Each modulated (simulated) differential intensity was obtained using a diffusion tensor (Sects. 2, 2.1, 4 and Appendix A), whose elements depend on the actual value of the diffusion parameter K_0 . Furthermore, the modulated spectra were derived from a LIS [Eqs. (30, 33)] whose normalization constant (J_0) depends on the experimental set of data (see discussion in Sect. 7.1). In addition, these differential intensities were calculated 1) for a polar-increased value of $K_{\perp\theta}$ [Eq. (8)] and also with $K_{\perp\theta} = K_{\perp r}$, and 2) accounting for particles inside two

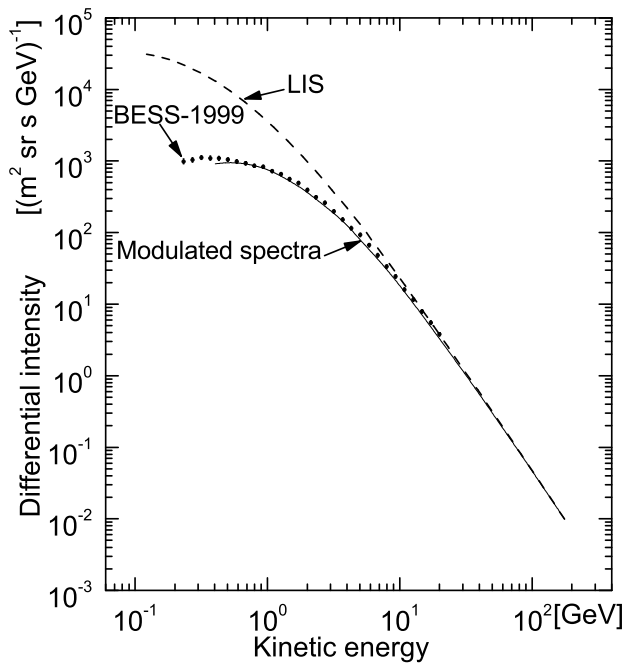


Fig. 4.— Differential intensity determined with HelMod code (continuous line) compared to the experimental data of BESS–1999; the dashed line is the LIS (see text).

heliospheric regions where solar latitudes are lower than $|5.7^\circ|$ and $|30^\circ|$, respectively. As discussed in Sect. 2.1, in the present model K_P is assumed to be equal to the value of the rigidity (P) [Eq. (7)] above proton kinetic energies of ≈ 444 MeV (e.g., Gloeckler & Jokipii 1966; Gleeson & Axford 1968; Perko 1987; Potgieter & Le Roux 1994). However, it has to be remarked that a systematic investigation of its dependence below that value and the shape of low energy part of the LIS spectrum [Eqs. (30, 33)] was not attempted using the modulated intensities obtained from HelMod code. In fact, this investigation is likely to be carried out using the experimental data from accurate observations over a long duration, like those from the AMS-02 spectrometer which will allow one to reconstruct the particle trajectory. The reconstructed particle trajectory results in untangling GCRs coming from outside the magnetosphere also at large geomagnetic latitudes (Θ_M) where less energetic particles can enter the magnetosphere. For instance, inside highest geomagnetic region with $1 < \Theta_M < 1.1$ radian [e.g., see Figure 2(c) in (Alcaraz et al. 2000a) and Figure 8 in (Bobik et al. 2006)] AMS-1998 data indicate that i) the effective geomagnetic cut-off prevents primary protons (i.e., CR protons) from being fully observed with energies below $\approx (0.5\text{--}0.6)$ GeV and ii) secondary particles largely contribute to the overall differential intensity. In addition, it has been noted that BESS observations were usually performed at large geomagnetic latitudes with Θ_M close to 1.13 radian.

The past period of high solar activity was during the solar cycle 23; BESS collaboration

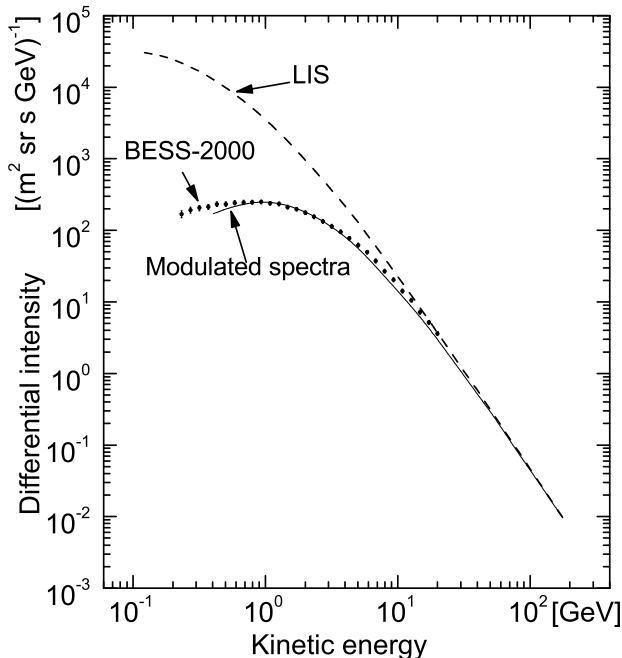


Fig. 5.— Differential intensity determined with HelMod code (continuous line) compared to the experimental data of BESS-2000; the dashed line is the LIS (see text).

took data in the years 1999, 2000 and 2002 [see sets of data in (Shikaze et al. 2007)]. These data were compared with those obtained by means of HelMod code using the error-weighted root mean square (η_{RMS}) of the relative difference (η) between experimental data (f_{exp}) and those resulting from simulated differential intensities (f_{sim}). For each set of experimental data and above described approximations and/or models, we determined the quantity:

$$\eta_{\text{RMS}} = \sqrt{\frac{\sum_i (\eta_i / \sigma_{\eta,i})^2}{\sum_i 1 / \sigma_{\eta,i}^2}} \quad (34)$$

with

$$\eta_i = \frac{f_{\text{sim}}(T_i) - f_{\text{exp}}(T_i)}{f_{\text{exp}}(T_i)}, \quad (35)$$

where T_i is the average energy of the i -th energy bin of the differential intensity distribution and $\sigma_{\eta,i}$ are the errors including the experimental and Monte Carlo uncertainties; the latter account for the Poisson error of each energy bin. The simulated differential intensities are interpolated with a cubic spline function.

In Tables 2, 3, the values of the parameter η_{RMS} (in percentage) are shown; they were

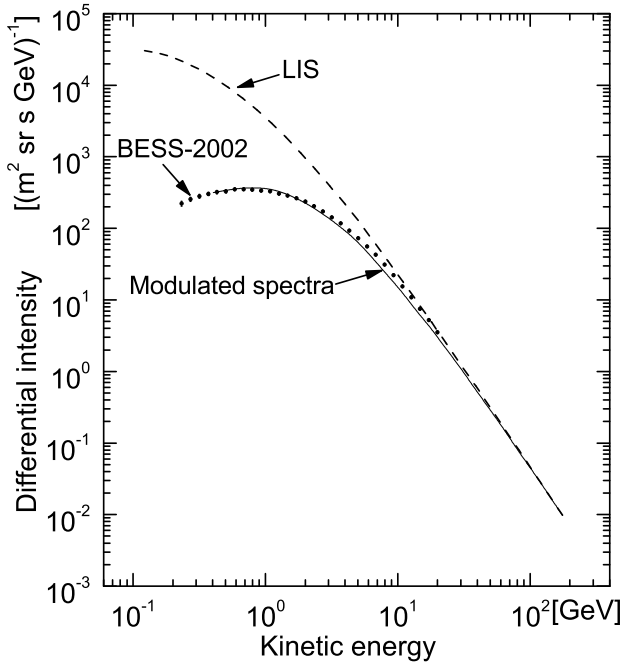


Fig. 6.— Differential intensity determined with HelMod code (continuous line) compared to the experimental data of BESS-2002; the dashed line is the LIS (see text).

obtained in the energy range⁷ from 444 MeV up to 30 GeV using “L” and “R” models for the tilt angle (α_t) [Sect. 5 and (Hoeksema 1995; WSO 2010)], for *no drift* approximation, *diagonal approximation* and *scalar approximation* (approximations discussed previously in this section), finally with (Table 2) and without (Table 3) the enhancement of the diffusion tensor along the polar direction ($K_{\perp\theta}$) [Eq. (8)]. The simulated differential intensity were obtained for a heliospheric region where solar latitudes are lower than $|30^\circ|$. From inspection of Tables 2 and 3, one can note that i) the *no drift approximation* is better appropriate than *diagonal* and *scalar approximations*, ii) the “L” model for calculating the values of tilt angle (α_t) is slightly to be preferred to “R” model (although the overall differences between these two models are marginal), iii) the results obtained accounting for drift effects using tilt angles from “L” model are better in agreement with experimental data with respect to the *no drift* approximation and, finally, iv) the minimum difference with the experimental data occurs when $K_{\perp\theta} = K_{\perp r}$ is assumed independently of the latitude (Table 3, see first column of the left-hand side). In addition, the results obtained for a heliospheric region where solar latitudes are lower than $|5.7^\circ|$ exhibit a behavior similar to those lower than $|30^\circ|$, but with values of η_{RMS} (in percentage) larger by about several percents. In Figs. 4, 5, 6 the

⁷Above 30 GeV the differential intensity is marginally (if at all) affected by modulation.

	“L” model	“R” model	<i>no drift</i>	<i>diagonal approx.</i>	<i>scalar approx.</i>
BESS–1997	9.2	17.7	10.4	9.5	17.6
AMS–1998	4.6	7.9	12.9	5.4	17.3
BESS–1998	9.1	14.1	9.3	4.7	13.6
PAMELA–2006/08	7.1	13.4	5.9	17.5	52.5

Table 4: For BESS–1997, AMS–1998, BESS–1998 and PAMELA–2006/08, η_{RMS} (in percentage) obtained from Eq. (34) *with enhancement of the diffusion tensor along the polar direction* using “L” and “R” models for the tilt angle and for *no drift* approximation, *diagonal approximation* and, finally, *scalar approximation* (see Sect. 7.2).

	“L” model	“R” model	<i>no drift</i>	<i>diagonal approx.</i>	<i>scalar approx.</i>
BESS–1997	13.4	20.6	14.2	11.13	12.0
AMS–1998	6.1	11.3	11.4	6.0	3.7
BESS–1998	11.1	17.7	7.3	4.1	7.1
PAMELA–2006/08	11.0	24.7	5.4	12.3	30.6

Table 5: For BESS–1997, AMS–1998, BESS–1998 and PAMELA–2006/08, η_{RMS} (in percentage) obtained from Eq. (34) *without any enhancement of the diffusion tensor along the polar direction* using “L” and “R” models for the tilt angle and for *no drift* approximation, *diagonal approximation* and, finally, *scalar approximation* (see Sect. 7.2).

differential intensities determined with HelMod code are shown and compared with the experimental data of BESS–1999, BESS–2000 and BESS–2002, respectively; in the same figures, the dashed line is the LIS [Eqs. (30, 33)] with normalization constants J_0 treated in Sect.7.1. These modulated intensities are the ones calculated for a heliospheric region where solar latitudes are lower than $|30^\circ|$, using $K_{\perp\theta} = K_{\perp r}$ independently of the latitude and including particle drift effects with the values of tilt angle from the “L” model.

Finally, it has be concluded that the present code combining diffusion and drift mechanisms is suited to describe the modulation effect in periods with high solar activity (e.g., see Ferreira & Potgieter 2004; Ndiitwani et al. 2005).

7.2.1. Periods not Dominated by High Solar Activity

In periods where the *solar activity is no longer at maximum*, the solar magnetic field becomes increasingly dipolar (Sects. 2, 3). We used the present code to compare the simu-

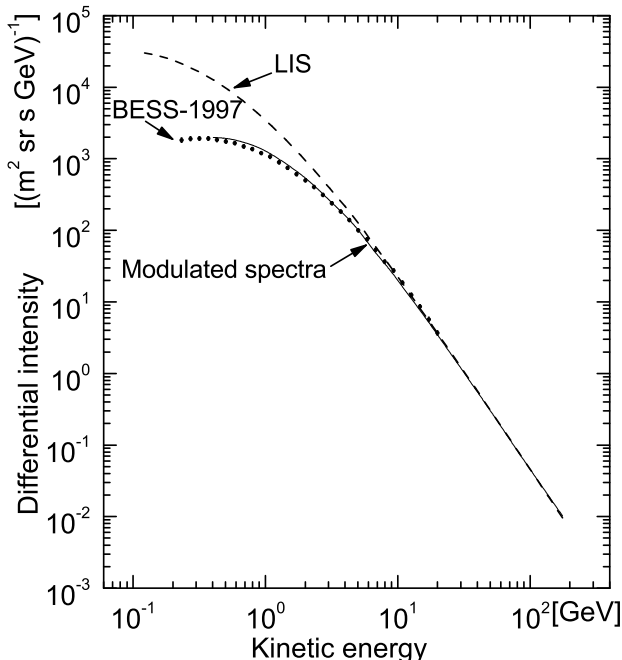


Fig. 7.— Differential intensity determined with HelMod code (continuous line) compared to the experimental data of BESS–1997; the dashed line is the LIS (see text).

lated differential intensities with experimental data obtained during periods not dominated by high solar activity in the solar cycle 23, i.e., BESS–1997 (Shikaze et al. 2007), AMS–1998 (Aguilar et al. 2002), BESS–1998 (Shikaze et al. 2007; Sanuki et al. 2000) and PAMELA–2006/08 (Adriani et al. 2011a). As discussed in Sect. 7.2, the simulated spectra were calculated including the effects due to particle drift - expected to be relevant (Sects. 2, 4) - with the value of tilt angles (α_t) calculated following the approach due to “R” and “L” models [Sect. 5 and (Hoeksema 1995; WSO 2010)], with and without the polar enhancement of the diffusion tensor along the polar direction ($K_{\perp\theta}$) [Eq. (8)]. Similarly to the treatment for periods with high solar activity (Sect. 7.2), the effects related to particle drift were also investigated (a) via the suppression of the drift velocity (*no drift*), (b) with the *diagonal approximation* and, finally, (c) with the *scalar approximation*.

In Tables 4 and 5, the values of the parameter η_{RMS} (in percentage) are shown. They were obtained in the energy range from 444 MeV up to 30 GeV using “L” and “R” models for the tilt angle (α_t) [Sect. 5 and (Hoeksema 1995; WSO 2010)], for *no drift* approximation, *diagonal approximation* and *scalar approximation* (approximations discussed in this Sect.7.2), finally with (Table 4) and without (Table 5) the enhancement of the diffusion tensor along the polar direction ($K_{\perp\theta}$) [Eq. (8)]. The simulated differential intensity were obtained for a heliospheric region where solar latitudes are lower than $|5.7^\circ|$. From inspection of Tables 4

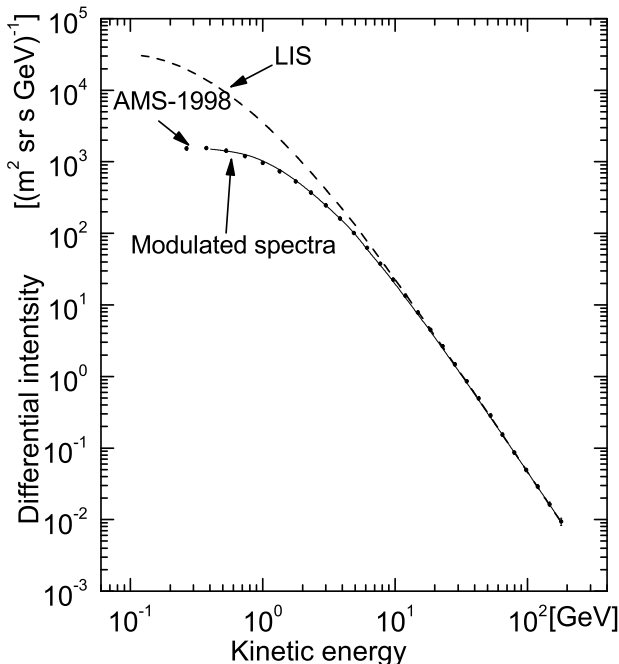


Fig. 8.— Differential intensity determined with HelMod code (continuous line) compared to the experimental data of AMS–1998; the dashed line is the LIS (see text).

and 5, one can note that i) the *diagonal approximation* is better appropriate than *no drift* and *scalar approximations*, ii) the “L” model for tilt angles (α_t) is slightly to be preferred to “R” model and, finally, iii) the minimum difference with the experimental data occurs when the enhancement of the diffusion tensor along the polar direction ($K_{\perp\theta}$) [Eq. (8)] is taken into account (Table 4, see first column of the left-hand side). In addition, the results obtained for a heliospheric region where solar latitudes are lower than $|30^\circ|$ exhibit a behavior similar to those lower than $|5.7^\circ|$, but with values of η_{RMS} (in percentage) larger by about several percents. In Figs. 7–10, the differential intensities determined with HelMod code are shown and compared to the experimental data of BESS–1997, AMS–1998, BESS–1998 and PAMELA–2006/08, respectively; in the same figures, the dashed line is the LIS [Eqs. (30, 33)] with normalization constants J_0 treated in Sect.7.1. These modulated intensities are the ones calculated for a heliospheric region where solar latitudes are lower than $|5.7^\circ|$, using the enhancement of the diffusion tensor along the polar direction ($K_{\perp\theta}$) [Eq. (8)] and including particle drift effects with the values of tilt angle from “L” model.

Finally, it has been concluded that the present code combining diffusion and drift mechanisms is also suited to describe the modulation effect in periods when the solar activity is no longer at the maximum.

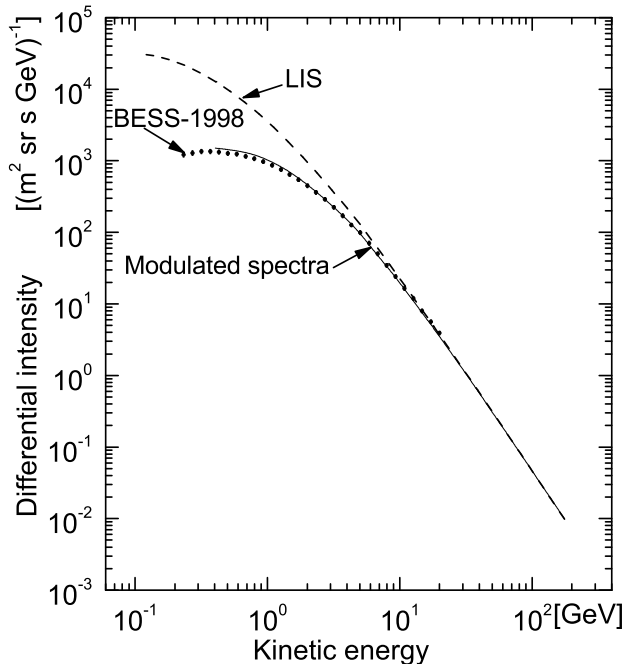


Fig. 9.— Differential intensity determined with HelMod code (continuous line) compared to the experimental data of BESS–1998; the dashed line is the LIS (see text).

7.3. Dependence on the Extension of Heliosphere

In Sects. 7.2 and 7.2.1, the simulated differential intensities were obtained from a LIS [described by Eqs. (30, 33)] propagating through a spherical heliosphere with a radius of 100 AU down to Earth. However, the physical dimensions of the heliosphere also depends on the speed of solar wind. In HelMod code, the simulated modulated intensities are determined by the properties of the diffusion tensor (Sects. 2, 2.1, 4 and Appendix A), whose elements are related to the actual value of the diffusion parameter. K_0 acts as a *scaling factor* for the overall modulation effect. It was indirectly determined from neutron monitor measurements, thus, it is expected to be sensitive to the overall modulation effect (from the heliosphere boundary down to Earth), but almost independent of the variation of heliosphere dimensions.

The radial distance of the heliosphere was varied from 80 up 120 AU. The corresponding simulated differential intensities were compared to the experimental data from BESS–2002 [data collected during high solar activity (Sect. 7.2)] and PAMELA–2006/08 [data collected when the solar activity was no longer large (Sect. 7.2.1)], i.e., when heliosphere is expected to be smaller or larger (and possibly no longer spherical) than 100 AU, respectively.

The values of η_{RMS} [Eq. (34)] in percentage calculated for spherical heliospheres with

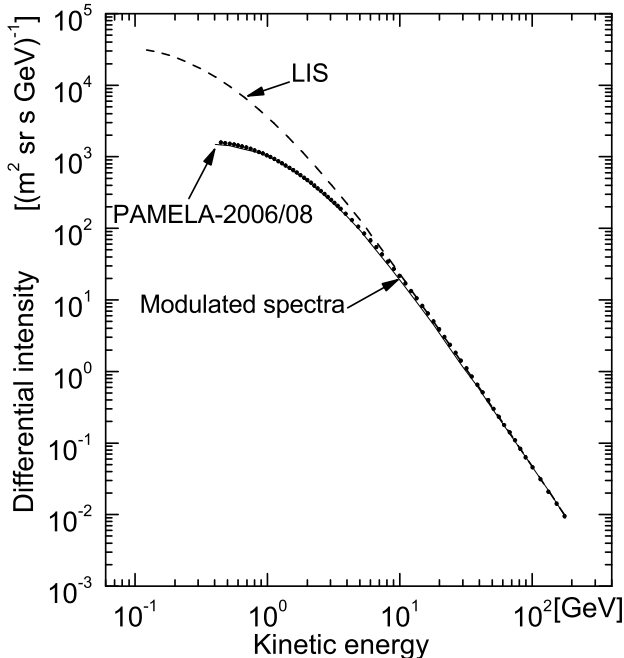


Fig. 10.— Differential intensity determined with HelMod code (continuous line) compared to the experimental data of PAMELA–2006/08; the dashed line is the LIS (see text).

radii of 80, 90, 110 and 120 AU are shown in Table 6 and compared with those calculated with a radius of 100 AU (see Tables 3, 4). For BESS–2002, the simulated intensities were obtained i) using the “L” model for the tilt angle (α_t) [Sect. 5 and (Hoeksema 1995; WSO 2010)], ii) with $K_{\perp\theta} = K_{\perp r}$ independently of the latitude and iii) inside a heliospheric region where solar latitudes are lower than $|30^\circ|$. For PAMELA–2006/08, the simulated intensities were obtained a) using the “L” model for the tilt angle (α_t) [Sect. 5 and (Hoeksema 1995; WSO 2010)], b) with an enhancement of the diffusion tensor along the polar direction ($K_{\perp\theta}$) [Eq. (8)] and c) inside a heliospheric region where solar latitudes are lower than $|5.7^\circ|$. From inspection of Table 6, one can remark that, within 2.3%, the simulated differential intensities for spherical heliospheres with radii of 80, 90 and 110 AU are compatible with that with a radius of 100 AU; slightly larger values of η_{RMS} were obtained for a spherical heliosphere with a radius of 120 AU.

The sensitivity of this approach was estimated from the differences of the simulated intensities with radii of 80, 90, 110 and 120 AU with that with a radius of 100 AU for protons with energies above 30 GeV, i.e., for an energy region in which the spectrum is unaffected by modulation and, thus, no difference is expected. For this purpose, we defined the quantity

[see also Eqs. (34, 35)]

$$\hat{\eta}_{\text{RMS,h}} = \sqrt{\frac{\sum_i (\hat{\eta}_{i,h}/\sigma_{\hat{\eta}_{i,h}})^2}{\sum_i 1/\sigma_{\hat{\eta}_{i,h}}^2}} \quad (36)$$

with

$$\hat{\eta}_{i,h} = \frac{f_h(T_i) - f_{100\text{AU}}(T_i)}{f_{100\text{AU}}(T_i)}, \quad (37)$$

where $f_h(T_i)$ is the differential intensity of i -th energy bin (above 30 GeV), $\sigma_{\hat{\eta}_{i,h}}$ is the error due to Monte Carlo uncertainties for i -th energy bin, $f_{100\text{AU}}(T_i)$ is the differential intensity computed with a radius of 100 AU and, finally “h” indicates 80, 90, 110 and 120 AU. $\hat{\eta}_{\text{RMS,h}}$ resulted equal to about 2.3% for heliospheres with 80, 90, 110 and 120 AU. Thus, the modulated intensities for heliospheres with radii of 80, 90, 100, 110 AU (and also 120 AU for BESS-2002) are in agreement among them and experimental data within the present sensitivity of about 2.3% of the current approach; at 120 AU the simulated intensity is marginally non compatible with that obtained with 100 AU for PAMELA–2006/08. These results indicated that, as expected, the diffusion parameter almost accounts for effects related to the variation of the physical dimensions of the heliosphere within the present approximations.

7.4. Dependence on Heliospheric Latitude

Observations made by the Ulysses spacecraft (Simpson et al. 1992) in the inner heliosphere could determine a latitudinal dependence of GCR (mostly protons) intensity with an equatorial southward offset minimum and a North polar excess. This dependence was discussed also in terms of modulation models which were including particle drift effects (e.g., see Simpson 1996; Heber et al. 1998). For protons with energies larger than 100 MeV, Simpson, Zhang and Bame (1996) expressed their results in terms of the solar latitude and found that i) the latitudinal gradient is $\approx (0.33 \pm 0.02)\% \text{ deg}^{-1}$, ii) the counting rate minimum is nearly constant in a latitudinal region of $\approx -(15^\circ - 5^\circ)$ [Figure 2 of Simpson, Zhang and Bame (1996)] at ≈ 1.35 AU [e.g., see (Simpson 1996; Heber et al. 1998)] and iii) the rate at the minimum is about $\approx 80\%$

	80 AU	90 AU	100 AU	110 AU	120 AU
BESS-2002	14.5	12.00	12.2	13.0	14.5
PAMELA–2006/08	5.7	6.1	7.1	7.7	10.8

Table 6: η_{RMS} (in percentage) calculated for a spherical heliosphere with radius of 80, 90, 110 and 120 AU and compared with those obtained with a radius of 100 AU: for BESS–2002 (see Table 3), for PAMELA–2006/08 (see Table 4).

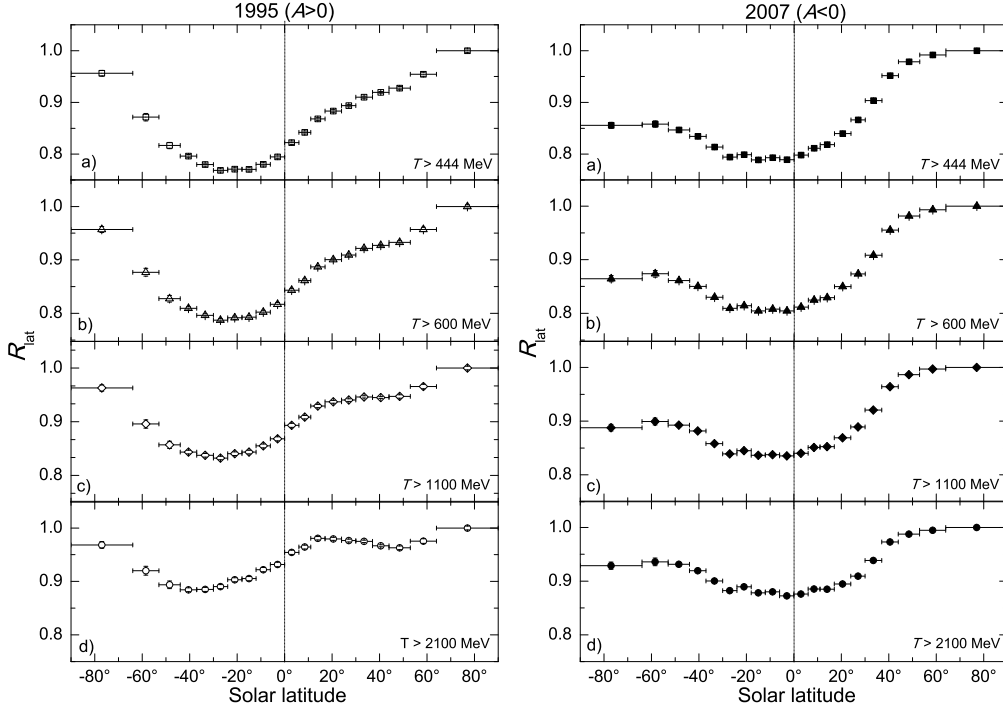


Fig. 11.— R_{lat} calculated at 1 AU as a function function of solar latitude for a) $T_e > 444$ MeV, b) $T_e > 600$ MeV, c) $T_e > 1200$ MeV and d) $T_e > 2100$ MeV: left-hand side during 1995 ($A > 0$), right-hand during 2007 ($A < 0$).

with respect to that at $\approx 80^\circ$. Ferreira et al. (2003) have shown that the latitudinal dip - found with the Ulysses fast scan - can be reproduced in a model using the Parker standard field and a polar enhancement of the diffusion tensor.

Using HelMod code, we could investigate the latitudinal dependence of the differential intensity at 1 AU, above 444 MeV (as so far treated) up to 200 GeV. The heliosphere was subdivided in 20 regions equally spaced with respect to the co-latitudinal parameter $\mu(\theta)$ [Sect. 6]. The total fluxes obtained in each region were divided by the maximum flux occurring at the North pole, thus, R_{lat} represents the normalized flux (to that at the North pole) as a function of the co-latitude. In addition, the values of R_{lat} were calculated for periods of opposite magnetic polarities and compatible with Ulysses pole-to-pole fast scans, i.e., for the years 1995 with $A > 0$ and 2007 with $A < 0$. R_{lat} can be equivalently expressed as a function of the solar latitude for a comparison with the results obtained by Simpson, Zhang and Bame (1996). R_{lat} as a function the solar latitude is shown in Fig. 11 for the year 1995 (left-hand side) and 2007 (right-hand side). R_{lat} is also shown as a function of the minimum kinetic energy accounted for protons (T_e), i.e., a) $T_e > 444$ MeV, b) $T_e > 600$ MeV, c) $T_e > 1100$ MeV and d) $T_e > 2100$ MeV. By inspection of Fig. 11, for the year 1995 one

can remark that R_{lat} has 1) a latitudinal gradient of $(0.23 \pm 0.01)\% \text{ deg}^{-1}$, 2) an equatorial southward offset minimum in the latitudinal region $\approx -(18^\circ-5^\circ)$ with $T_e > 444 \text{ MeV}$ and 3) at this minimum, the flux is about $\approx 80\%$ of that at the North pole. Thus, the simulated fluxes reproduce the features of the experimental data (above 100 MeV) exhibited in Figures 2 and 3 of Simpson, Zhang and Bame (1996) [see also (Heber et al. 2008)] regarding the period of 1995 Ulysses fast scan. However with increasing T_e , the latitudinal gradient decreases (Fig. 11, left-hand side). In the year 2007, a similar minimum is exhibited for $T_e > 444 \text{ MeV}$ with a $\approx 10\%$ North–South poles asymmetry; with increasing T_e , this asymmetry gradually disappears and the flux reduction on the equatorial region is less pronounced down to $\approx 88\%$ with $T_e > 2100 \text{ MeV}$ (Fig. 11, right-hand side).

It is worthwhile to note that in HelMod code the magnetic field structure is treated similarly in North and South hemisphere approximating Parker’s magnetic-field with that suggested by Kóta & Jokipii (1989) (Sect. 3). However, the current 2-D model uses the complete 2×2 diffusion tensor (see Sects. 3, 6 and Appendix A) which contains both symmetric and antisymmetric components in the off-diagonal terms. The symmetric component of the off-diagonal terms [Eq. (A13)] is determined by the divergence-free IMF used, which exhibits a latitudinal component arising from the modification by Kóta & Jokipii (1989) [Eqs. (15, 18, 19)]. In the framework of the present 2-D model, the North polar excess and equatorial southward offset minimum shown in Fig. 11 originate from the non-zero symmetric component of the off-diagonal terms. The actual extension of the dip is related to both the enhancement of the diffusion tensor in the polar regions [Eq. (8)] and drift effects.

8. Conclusions

A systematic investigation of the solar modulation effect on the propagation of cosmic protons through the heliosphere down to the Earth was carried out comparing experimental observations performed during the solar cycle 23 and simulated differential intensities obtained using HelMod code. The simulated spectra were derived from a LIS [Eqs. (30, 33)], whose normalization constant (J_0) depends on the experimental set of data (see discussion in Sect.7.1). The stochastic 2D Monte Carlo (HelMod) code includes i) a fully treated diffusion tensor with symmetric and antisymmetric off-diagonal elements, b) a diffusion parameter which is a function of the intensity of solar activity and varies with solar polarity and phase (Sects. 2.1, 5) and c) a magnetic-field which is modified with respect to Parker’s magnetic field in the polar region as proposed by Kóta & Jokipii (1989) (Sect. 3).

For observations performed during high solar activity, the simulated intensities (found with a better agreement to experimental data) were obtained i) using the “L” model for the

tilt angle (α_t) [Sect. 5 and (Hoeksema 1995; WSO 2010)], ii) with $K_{\perp\theta} = K_{\perp r}$ independently of the latitude and iii) inside a heliospheric region where solar latitudes are lower than $|30^\circ|$. For observations performed when solar activity is no longer at the maximum, the simulated intensities (found with a better agreement to experimental data) were obtained a) using the “L” model for the tilt angle (α_t) [Sect. 5 and (Hoeksema 1995; WSO 2010)], b) with an enhancement of the diffusion tensor along the polar direction ($K_{\perp\theta}$) [Eq. (8)] and c) inside a heliospheric region where solar latitudes are lower than $|5.7^\circ|$.

In addition (within 2.3%), the simulated differential intensities for spherical heliospheres with radii of 80, 90 and 110 AU (and also 120 AU for BESS-2002) are compatible with that with a radius of 100 AU; a slightly lower agreement was obtained for a spherical heliosphere with a radius of 120 AU for PAMELA–2006/2008. These results indicated that, within the present approximations, the diffusion parameter almost accounts for effects related to the variation of the physical dimensions of the heliosphere.

The simulated modulated spectrum determined for the year 1995 exhibits a latitudinal gradient of $(0.23 \pm 0.01)\% \text{ deg}^{-1}$, an equatorial southward offset minimum in the latitudinal region $\approx -(18^\circ-5^\circ)$ with $T_e > 444 \text{ MeV}$ and at this minimum the flux is about $\approx 80\%$ of that at North pole. Thus, the simulated fluxes reproduce the features of the experimental data from Ulysses fast scan in 1995 (Simpson, Zhang and Bame 1996).

Although the treatment is highly simplified with respect to the complexity of physical mechanisms responsible for modulation effects, the overall satisfactory agreement found allows one to remark that the choice of parameters regarding the structure of IMF, diffusion tensor, diffusion parameter and tilt angle is almost appropriate to describe the experimental data. Finally, the experimental data from accurate observations over a long duration (like those from the AMS-02 spectrometer) will allow one to undertake a deeper systematic investigation of solar modulation effects over a period longer than a solar cycle. Thus, possibly, further advancements can be put forward in the present approximations on the transport of GCR’s through the heliosphere, for instance those at low rigidities, the spatial and rigidity properties of diffusion tensor.

Appendix

A. Diffusion Tensor and Stochastic Differential Equations

In a reference frame with the 3rd coordinates along the average magnetic field, the matrix of the diffusion tensor used in Eqs. (1, 4) is given by (e.g., see Jokipii 1971):

$$K_{ik} = \begin{vmatrix} K_{\perp r} & -K_A & 0 \\ K_A & K_{\perp \theta} & 0 \\ 0 & 0 & K_{\parallel} \end{vmatrix}.$$

In heliocentric spherical coordinates (r, θ, ϕ) , for instance those used in Eqs. (A25–A27), the matrix elements of the 3×3 tensor are found, for instance, in Equation (17) of Burger et al. (2008). In a 2-D approximation, the matrix elements of the resulting tensor are:

$$K_{rr} = K_{\perp \theta} \sin^2 \xi + \cos^2 \xi (K_{\parallel} \cos^2 \psi + K_{\perp r} \sin^2 \psi), \quad (\text{A1})$$

$$K_{\theta\theta} = K_{\perp \theta} \cos^2 \xi + \sin^2 \xi (K_{\parallel} \cos^2 \psi + K_{\perp r} \sin^2 \psi), \quad (\text{A2})$$

$$K_{r\theta} = -K_A \sin \psi + \sin \xi \cos \xi (K_{\parallel} \cos^2 \psi + K_{\perp r} \sin^2 \psi - K_{\perp \theta}), \quad (\text{A3})$$

$$K_{\theta r} = K_A \sin \psi + \sin \xi \cos \xi (K_{\parallel} \cos^2 \psi + K_{\perp r} \sin^2 \psi - K_{\perp \theta}) \quad (\text{A4})$$

with $\tan \psi = -B_{\phi}/(\sqrt{B_r^2 + B_{\theta}^2})$ and $\tan \xi = B_{\theta}/B_r$ [see Figure 6 of Burger et al. (2008)], where ψ is the spiral angle (for a standard Parker IMF $\tan \psi$ reduces to Eq. (16) and $\tan \xi = 0$), and with

$$K_{\parallel} = \beta k_1(r, t) K_P(P, t) \left[\frac{B_{\oplus}}{3B} \right], \quad (\text{A5})$$

$$K_{\perp r} = \rho_k K_{\parallel}, \quad (\text{A6})$$

$$K_{\perp \theta} = \iota(\theta) \rho_k K_{\parallel}, \quad (\text{A7})$$

where $\rho_k = 0.05$ and $\iota(\theta)$ is a step function that is 1 in equatorial region and 10 in polar region (Sect. 2). The diffusion parameter $k_1(r, t)$ is replaced by K_0 for an effective heliosphere of 100 AU (Sect. 2.1). Furthermore, the matrix elements of the later tensor consist of a symmetric (K_{ik}^S) and antisymmetric (K_{ik}^A) part:

$$K_{ik} = K_{ik}^A + K_{ik}^S \quad (\text{A8})$$

with the antisymmetric part related to drift velocity [Eq. (22)], \vec{v}_d , and treated in Sect. 4. Finally, using Eqs. (A5–A8), Eqs. (A1–A4) can be re-written as:

$$K_{rr} = K_{rr}^S = \beta K_0 K_P(P, t) \left[\frac{B_{\oplus}}{3B} \right] [\iota(\theta) \rho_k \sin^2 \xi + \cos^2 \xi (\cos^2 \psi + \rho_k \sin^2 \psi)], \quad (\text{A9})$$

$$K_{\theta\theta} = K_{\theta\theta}^S = \beta K_0 K_P(P, t) \left[\frac{B_{\oplus}}{3B} \right] [\iota(\theta)\rho_k \cos^2 \xi + \sin^2 \xi (\cos^2 \psi + \rho_k \sin^2 \psi)], \quad (\text{A10})$$

$$K_{r\theta} = K_{r\theta}^A + K_{r\theta}^S, \quad (\text{A11})$$

$$K_{\theta r} = K_{\theta r}^A + K_{\theta r}^S \quad (\text{A12})$$

with

$$K_{r\theta}^S = \beta K_0 K_P(P, t) \left[\frac{B_{\oplus}}{3B} \right] \{ \sin \xi \cos \xi [\cos^2 \psi + \rho_k \sin^2 \psi - \iota(\theta)\rho_k] \}, \quad (\text{A13})$$

$$K_{\theta r}^A = -K_{r\theta}^A = K_A \sin \psi. \quad (\text{A14})$$

Equations (1, 4) can be re-expressed in heliocentric spherical coordinates as:

$$\begin{aligned} \frac{\partial U}{\partial t} = & \frac{1}{r^2} \frac{\partial}{\partial r} \left(r^2 K_{rr}^S \frac{\partial}{\partial r} U + r K_{r\theta}^S \frac{\partial}{\partial \theta} U + \frac{r}{\sin \theta} K_{r\phi}^S \frac{\partial}{\partial \phi} U \right) \\ & + \frac{1}{r \sin \theta} \frac{\partial}{\partial \theta} \left(\sin \theta K_{\theta r}^S \frac{\partial}{\partial r} U + \frac{\sin \theta}{r} K_{\theta\theta}^S \frac{\partial}{\partial \theta} U + \frac{1}{r^2} K_{\theta\phi}^S \frac{\partial}{\partial \phi} U \right) \\ & + \frac{1}{r \sin \theta} \frac{\partial}{\partial \phi} \left(K_{\phi r}^S \frac{\partial}{\partial r} U + \frac{1}{r} K_{\phi\theta}^S \frac{\partial}{\partial \theta} U + \frac{1}{r \sin \theta} K_{\phi\phi}^S \frac{\partial}{\partial \phi} U \right) \\ & - \frac{1}{r^2} \frac{\partial r^2 V_r U}{\partial r} - \frac{1}{r \sin \theta} \frac{\partial \sin \theta V_{\theta} U}{\partial \theta} - \frac{1}{r \sin \theta} \frac{\partial V_{\phi} U}{\partial \phi} \\ & - \frac{1}{r^2} \frac{\partial r^2 v_{d,r} U}{\partial r} - \frac{1}{r \sin \theta} \frac{\partial \sin \theta v_{d,\theta} U}{\partial \theta} - \frac{1}{r \sin \theta} \frac{\partial v_{d,\phi} U}{\partial \phi} \\ & + \frac{1}{3} \left(\frac{1}{r^2} \frac{\partial r^2 V_r}{\partial r} + \frac{1}{r \sin \theta} \frac{\partial \sin \theta V_{\theta}}{\partial \theta} + \frac{1}{r \sin \theta} \frac{\partial V_{\phi}}{\partial \phi} \right) \frac{\partial}{\partial T} (\alpha_{\text{rel}} T U), \end{aligned} \quad (\text{A15})$$

where U is the number density of GCRs (Sect. 2) and T is the kinetic energy. In turn, in a 2-D (radial distance and co-latitude) approximation, Eq. (A15) can be re-expressed as:

$$\begin{aligned} \frac{\partial U}{\partial t} = & \frac{1}{r^2} \frac{\partial}{\partial r} \left(r^2 K_{rr}^S \frac{\partial}{\partial r} U + r K_{r\theta}^S \frac{\partial}{\partial \theta} U \right) + \frac{1}{r \sin \theta} \frac{\partial}{\partial \theta} \left(\sin \theta K_{\theta r}^S \frac{\partial}{\partial r} U + \frac{\sin \theta}{r} K_{\theta\theta}^S \frac{\partial}{\partial \theta} U \right) \\ & - \frac{1}{r^2} \frac{\partial r^2 V_r U}{\partial r} - \frac{1}{r \sin \theta} \frac{\partial \sin \theta V_{\theta} U}{\partial \theta} - \frac{1}{r^2} \frac{\partial r^2 v_{d,r} U}{\partial r} - \frac{1}{r \sin \theta} \frac{\partial \sin \theta v_{d,\theta} U}{\partial \theta} \\ & + \frac{1}{3} \left(\frac{1}{r^2} \frac{\partial r^2 V_r}{\partial r} + \frac{1}{r \sin \theta} \frac{\partial \sin \theta V_{\theta}}{\partial \theta} \right) \frac{\partial}{\partial T} (\alpha_{\text{rel}} T U). \end{aligned} \quad (\text{A16})$$

Let us define the variable $\mu = \cos(\theta)$, then we obtain

$$\partial \theta = -(1 - \mu^2)^{-0.5} \partial \mu. \quad (\text{A17})$$

In addition, one can introduce the function

$$F = U r^2. \quad (\text{A18})$$

Using Eqs. (A16–A18), for a SW radially propagating (i.e. $V_{\text{sw},r} = V_{\text{sw}}$) we find:

$$\begin{aligned} \frac{\partial F}{\partial t} = & -\frac{\partial}{\partial r} \left[\frac{F}{r^2} \frac{\partial}{\partial r} (r^2 K_{rr}^S) \right] - \frac{\partial}{\partial r} \left[-F \frac{\partial}{\partial \mu} \left(\frac{K_{r\theta}^S \sqrt{1-\mu^2}}{r} \right) \right] - \frac{\partial}{\partial r} [F(V_{\text{sw}} + v_{d,r})] \\ & - \frac{\partial}{\partial \mu} \left[-\frac{F}{r^2} \frac{\partial}{\partial r} (r K_{\theta r}^S \sqrt{1-\mu^2}) \right] - \frac{\partial}{\partial \mu} \left\{ F \frac{\partial}{\partial \mu} \left[\frac{K_{\theta\theta}^S (1-\mu^2)}{r^2} \right] \right\} \\ & - \frac{\partial}{\partial \mu} \left[-F \frac{v_{d,\theta} \sqrt{1-\mu^2}}{r} \right] - \frac{\partial}{\partial T} \left[-F \frac{\alpha_{\text{rel}} T}{3r^2} \frac{\partial V_{\text{sw}} r^2}{\partial r} \right] \\ & + \frac{1}{2} \frac{\partial}{\partial r} \frac{\partial}{\partial r} [2K_{rr}^S F] + \frac{1}{2} \frac{\partial}{\partial r} \frac{\partial}{\partial \mu} \left[-\frac{2K_{r\theta}^S \sqrt{1-\mu^2}}{r} F \right] \\ & + \frac{1}{2} \frac{\partial}{\partial \mu} \frac{\partial}{\partial r} \left[-\frac{2K_{\theta r}^S \sqrt{1-\mu^2}}{r} F \right] + \frac{1}{2} \frac{\partial}{\partial \mu} \frac{\partial}{\partial \mu} \left[\frac{2K_{\theta\theta}^S (1-\mu^2)}{r^2} F \right]. \end{aligned} \quad (\text{A19})$$

Furthermore, following the treatment discussed in Sections 4.3–4.3.5 of (Gardiner 1985), one can a) express the Fokker-Plank equation involving F - which, in turn, is a function of $\mathbf{q} = (r, \mu, T)$ - as:

$$\frac{\partial}{\partial t} F = - \sum_i \frac{\partial}{\partial q_i} [A_i(\mathbf{q}, t) F] + \frac{1}{2} \sum_{i,j} \frac{\partial}{\partial q_i} \frac{\partial}{\partial q_j} \{ [\tilde{\mathbf{D}}(\mathbf{q}, t)]_{ij} F \} \quad (\text{A20})$$

with $\tilde{\mathbf{D}} = \tilde{\mathbf{L}}\tilde{\mathbf{L}}^T$ and b) obtain the equivalent set of differential equations

$$d\mathbf{q} = \mathbf{A}(\mathbf{q}, t) dt + \tilde{\mathbf{L}}(\mathbf{q}, t) d\mathbf{W}(t), \quad (\text{A21})$$

where $\mathbf{A}(\mathbf{q}, t) dt$ accounts for the so-called *advective processes* (e.g., Kruells & Achterberg 1994), $\tilde{\mathbf{L}}(\mathbf{q}, t) d\mathbf{W}(t)$ is the *stochastic term* containing $d\mathbf{W}(t)$ which is the increment of the so-called *Wiener process* (e.g., Section 4.3 of Gardiner 1985). Equations (A21) are termed *stochastic differential equations* (SDEs).

Furthermore, one can note that i) the first right-hand term of Eq. (A20) is equal to those included in the first three lines of Eq. (A19) and ii) the second right-hand term of Eq. (A20) is equal to those included in the fourth and fifth line of Eq. (A19). Thus, using Eqs. (A19, A20) one derives:

$$\mathbf{A} = \left[\begin{array}{c} \frac{1}{r^2} \frac{\partial}{\partial r} (r^2 K_{rr}^S) - \frac{\partial}{\partial \mu} \left(\frac{K_{r\theta}^S \sqrt{1-\mu^2}}{r} \right) + V_{\text{sw}} + v_{d,r} \\ -\frac{1}{r^2} \frac{\partial}{\partial r} (r K_{\theta r}^S \sqrt{1-\mu^2}) + \frac{\partial}{\partial \mu} \left[\frac{K_{\theta\theta}^S (1-\mu^2)}{r^2} \right] - \frac{v_{d,\theta} \sqrt{1-\mu^2}}{r} \\ -\frac{\alpha_{\text{rel}} T}{3r^2} \frac{\partial V_{\text{sw}} r^2}{\partial r} \end{array} \right] \quad (\text{A22})$$

and

$$\tilde{\mathbf{D}} = \begin{bmatrix} 2K_{rr}^S & -\frac{2K_{r\theta}^S\sqrt{1-\mu^2}}{r} \\ -\frac{2K_{\theta r}^S\sqrt{1-\mu^2}}{r} & \frac{2K_{\theta\theta}^S(1-\mu^2)}{r^2} \end{bmatrix}. \quad (\text{A23})$$

As discussed by Pei et al. (2010b) - see Section 2 therein -, the matrix $\tilde{\mathbf{D}}$ can be downgraded to a two-by-two matrix, because second order acceleration mechanisms are not considered in Eqs. (1, 4).

As already shown by Pei et al. (2010b) - see Appendix B therein -, the matrix $\tilde{\mathbf{L}}$ is not unique. However, there is only one positive definite, i.e.,

$$\tilde{\mathbf{L}} = \begin{bmatrix} \left[\frac{K_{rr}^S K_{\theta\theta}^S - (K_{r\theta}^S)^2}{0.5K_{\theta\theta}^S} \right]^{1/2} & -K_{r\theta}^S \left(\frac{2}{K_{\theta\theta}^S} \right)^{1/2} \\ 0 & \left[\frac{2K_{\theta\theta}^S(1-\mu^2)}{r^2} \right]^{1/2} \end{bmatrix}. \quad (\text{A24})$$

Finally, for a 2-dimensional model (like that treated in Sects. 3, 4), from Eqs. (A21, A22) and using Eq. (A24) one finds the following SDEs:

$$\begin{aligned} dr &= \left[\frac{1}{r^2} \frac{\partial}{\partial r} (r^2 K_{rr}^S) - \frac{\partial}{\partial \mu} \left(\frac{K_{r\theta}^S \sqrt{1-\mu^2}}{r} \right) + V_{\text{sw}} + v_{d,r} \right] dt + \\ &+ \sqrt{\frac{K_{rr}^S K_{\theta\theta}^S - (K_{r\theta}^S)^2}{0.5K_{\theta\theta}^S}} dW_r - K_{r\theta}^S \sqrt{\frac{2}{K_{\theta\theta}^S}} dW_\mu, \end{aligned} \quad (\text{A25})$$

$$\begin{aligned} d\mu &= \left\{ -\frac{1}{r^2} \frac{\partial}{\partial r} (r K_{\theta r}^S \sqrt{1-\mu^2}) + \frac{\partial}{\partial \mu} \left[\frac{K_{\theta\theta}^S(1-\mu^2)}{r^2} \right] - \frac{v_{d,\theta} \sqrt{1-\mu^2}}{r} \right\} dt + \\ &+ \sqrt{\frac{2K_{\theta\theta}^S(1-\mu^2)}{r^2}} dW_\mu, \end{aligned} \quad (\text{A26})$$

$$dT = -\frac{2}{3} \frac{\alpha_{\text{rel}} V_{\text{sw}} T}{r} dt \quad (\text{A27})$$

with dW_i [$i = r, \mu(\theta)$] the increment of the Wiener process. It has be remarked that the above usage of Eq. (A24) ensures imaginary terms do not appear in Eqs. (A25–A30). For an IMF described by a standard Parker field [Eq. (15)] requiring $K_{r\theta}^S = 0$, the above SDEs reduce to

$$\begin{aligned} dr &= \frac{1}{r^2} \left[\frac{\partial}{\partial r} (r^2 K_{rr}^S) \right] dt + (V_{\text{sw}} + v_{d,r}) dt + \sqrt{2K_{rr}^S} dW_r, \\ d\mu &= \frac{1}{r^2} \left\{ \frac{\partial}{\partial \mu} [(1-\mu^2) K_{\theta\theta}^S] \right\} dt - \frac{v_{d,\theta} \sqrt{1-\mu^2}}{r} dt \end{aligned} \quad (\text{A28})$$

$$+ \sqrt{\frac{2 K_{\theta\theta}^S (1 - \mu^2)}{r^2}} dW_\mu, \quad (\text{A29})$$

$$dT = -\frac{2}{3} \frac{\alpha_{\text{rel}} V_{\text{sw}} T}{r} dt. \quad (\text{A30})$$

Gardiner (1985) - see Section 4.3.1 therein - demonstrated that, following a *Euler–Cauchy procedure*, the SDEs can be approximated in terms of the increments Δr , $\Delta\mu$ and ΔT occurring after a time Δt has elapsed. The corresponding increment of the Wiener Process is given by $\omega_i \sqrt{\Delta t}$ [with $i = r, \mu(\theta)$], where ω_i is a random number following a Gaussian distribution with a mean of zero and a standard deviation of one (e.g., see Kruells & Achterberg 1994 and appendix A of Pei et al. 2010b). As a consequence, the SDEs [Eqs. (A25–A27)] can be approximated by:

$$\begin{aligned} \Delta r = & \left[\frac{1}{r^2} \frac{\partial}{\partial r} (r^2 K_{rr}^S) - \frac{\partial}{\partial \mu} \left(\frac{K_{r\theta}^S \sqrt{1 - \mu^2}}{r} \right) + V_{\text{sw}} + v_{\text{dr},r} + v_{\text{HCS}} \right] \Delta t + \\ & + \omega_r \sqrt{\frac{K_{rr}^S K_{\theta\theta}^S - (K_{r\theta}^S)^2}{0.5 K_{\theta\theta}^S}} \Delta t - \omega_\mu K_{r\theta}^S \sqrt{\frac{2}{K_{\theta\theta}^S}} \Delta t, \end{aligned} \quad (\text{A31})$$

$$\begin{aligned} \Delta \mu = & \left\{ -\frac{1}{r^2} \frac{\partial}{\partial r} (r K_{\theta r}^S \sqrt{1 - \mu^2}) + \frac{\partial}{\partial \mu} \left[\frac{K_{\theta\theta}^S (1 - \mu^2)}{r^2} \right] - \frac{v_{\text{dr},\theta} \sqrt{1 - \mu^2}}{r} \right\} \Delta t + \\ & + \omega_\mu \sqrt{\frac{2 K_{\theta\theta}^S (1 - \mu^2)}{r^2}} \Delta t, \end{aligned} \quad (\text{A32})$$

$$\Delta T = -\frac{2}{3} \frac{\alpha_{\text{rel}} V_{\text{sw}} T}{r} \Delta t. \quad (\text{A33})$$

Acknowledgements

The authors express recognition for the contribution of Francesco Noventa to simulations regarding the heliosphere dimensions. KK wishes to acknowledge VEGA grant agency project 2/0081/10 for support. Finally, we acknowledge the use of NASA/GSFC’s Space Physics Data Facility’s OMNIWeb service, and OMNI data.

REFERENCES

- Abdo, A.A., et al., 2009, Phys. Rev. Lett., 102, id. 181101
 Abe, K., et al., 2008, Phys. Lett. B, 670, 103–108

- Achterberg, A., & Krulls, W.M., 1992. *A&A*, 265, L13–L16
- Adriani, O., et al., 2009a, *Nature*, 458, 607–609
- Adriani, O., et al., 2009b, *Phys. Rev. Lett.*, 102, id. 051101.
- Adriani, O., et al., 2010, *Phys. Rev. Lett.*, 105, id. 121101
- Adriani, O. et al., 2011a, *Science*, Published online 3 March, <http://www.sciencemag.org/content/early/2011/03/02/science.1199172.abstract>
- Adriani, O. et al., 2011b, *Science*, Published online 3 March, <http://www.sciencemag.org/cgi/content/full/science.1199172/DC1>
- Aguilar, M., et al., 2002, *Phys. Rep.*, 366, 331–405
- Aguilar, M., et al., 2007, *Phys. Lett. B*, 646, 145–154
- Alanko K.M., Usoskin I.G., Mursula K., & Kovaltsov G.A. 2003, in *Proc. of the 28th IICRC*, ed. Kajita, T., Asaoka, Y., Kawachi, A., Matsubara, Y. & Sasaki, M., 3851
- Alcaraz, J., et al., 2000a, *Phys. Lett. B*, 472, 215–226
- Alcaraz, J., et al., 2000b, *Phys. Lett. B*, 484, 10–22
- Alcaraz, J., et al., 2000c, *Phys. Lett. B*, 490, 27–35
- Alcaraz, J., et al., 2000d, *Phys. Lett. B*, 494, 193–202
- Armstrong, T.P., Pesses, M.E., & Decker, R.B., 1985, in *Collisionless Shocks in the Heliosphere: Reviews of Current Research*, ed. Tsuratani, B.T. & Stone, R.G. (Washington, D.C.: AGU), 271–285
- Aschwanden, M.J., 2006. *The Sun*, *Encyclopedia of the Solar System* (San Diego: Academic Press)
- Axford, W. I., 1965, *Planet. Space Sci.*, 13, 115–130
- Battiston, R., 2010, *Proc. of the 11th ICATPP*, ed. Leroy, C., Rancoita, P.G., Barone, M., Gaddi, A., Price, L. & Ruchti, R., (Singapore: World Scientific), 741–750
- Bobik, P., Gervasi, M., Grandi, D., Rancoita, P.G., & Usoskin, I.G. 2003, in *Solar variability as an input to the Earth’s environment. International Solar Cycle Studies (ISCS) Symposium*, ed.: A. Wilson (Noordwijk: ESA Publications Division), 637–640

- Bobik, P., Boella, G., Boschini, M.J., Gervasi, M., Grandi, D., Kudela, K., Pensotti S., & Rancoita, P.G. 2006, *J. Geophys. Res.*, 111, A05205
- Bobik, P., Boschini, M.J., Gervasi, M., Grandi, D., & Rancoita, P.G. 2008, *Proc. of the 10th ICATPP*, ed. Leroy, C., Rancoita, P.G., Barone, M., Gaddi, A., Price, L. & Ruchti, R., (Singapore: World Scientific), 881–885
- Bobik, P., Kudela, K., Boschini, M.J., Grandi, D., Gervasi, M. & Rancoita, P.G., 2008b, *Adv. in Sp. Res.*, 41, 229
- Bobik, P., Boschini, M.J., Della Torre, S., Gervasi, M., Grandi, D., Kudela, K., & Rancoita, P.G. 2010a, *Proc. of the 11th ICATPP*, ed. Leroy, C., Rancoita, P.G., Barone, M., Gaddi, A., Price, L. & Ruchti, R., (Singapore: World Scientific), 210–219
- Bobik, P., et al. 2010b, *Proc. Conf.: Proc. of the 11th ICATPP*, ed. Leroy, C., Rancoita, P.G., Barone, M., Gaddi, A., Price, L. & Ruchti, R., (Singapore: World Scientific), 760–764
- Bobik, P., et al. 2011a, *Proc. of the 12th ICATPP Conference on Cosmic Rays for Particle and Astroparticle Physics*, ed. Giani, S. Leroy, C. & Rancoita, P.G. (Singapore: World Scientific), 360–368 and (arXiv:1012.3086)
- Bobik, P., et al. 2011b, *Proc. of the ICATPP Conference on Cosmic Rays for Particle and Astroparticle Physics*, ed. C. Leroy, P.G. Rancoita, M. Barone, A. Gaddi, L. Price & R. Ruchti (Singapore: World Scientific), 337–342 and (arXiv:1011.4843)
- Bobik, P., et al. 2011c, *Proc. of the 12th ICATPP Conference on Cosmic Rays for Particle and Astroparticle Physics*, ed. Giani, S. Leroy, C. & Rancoita, P.G. (Singapore: World Scientific), 482–489
- Bobik, P. et al., 2011d, *Astrophys. Space Sci. Trans.*, 7, 245–249, doi:10.5194/astra-7-245-2011 and (arXiv:1102.0215)
- Boella, G., Gervasi, M., Potenza, M.A.C., Rancoita, P.G. & Usoskin, I.G., 1998, *Astropart. Phys.*, 9, 261–267
- Boella, G., Gervasi, M., Mariani, S., Rancoita, P.G., & Usoskin, I.G., 2001, *J. Geophys. Res.*, 106, 29355–29362
- Boezio, GM., et al., 1999, *ApJ*, 518, 457–472
- Bottino, A., Donato, F., Fornengo, N. & Salati, P., 1998, *Phys. Rev. D*, 58, 123503

- Brajša, R., Vršnak, B., Ruždjak, V., Roša, D., Hržina, D., Wöhl, H., Clette, F., Hochedez, J.-F. 2001, in *Recent Insights into the Physics of the Sun and Heliosphere*, Proc. of IAU Symposium 203, edited by P.Brekke, B. Fleck, & J.B. Gurman (San Francisco, Astronomical Society of the Pacific), 377
- Bravo, S., Stewart, G.A. & Blanconano, X., 1998, *Sol. Phys.*, 179, 223–235
- Burger, R.A., & Hattingh, M., 1995, *Ap&SS*, 230, 375–382
- Burger, R.A., & M.S. Potgieter 1989, *ApJ*, 339, 501–511
- Burger, R.A., Moraal, H. & Webb, G.M., 1985, *Ap&SS*, 116, 107–129
- Burger, R.A., Potgieter, M.S. & Heber, B., 2000, *J. Geophys. Res.*, 105, 27447–27455
- Burger, R.A., Krüger, T.P.J., Hitge, M., & Engelbrecht, N.E., 2008, *ApJ*, 674, 511–519
- Caballero-Lopez, R.A. & Moraal, H., 2004, *J. Geophys. Res.*, 109, A01101
- Cernuda, I., 2011, *Proc. of the 12th ICATPP Conference on Cosmic Rays for Particle and Astroparticle Physics*, ed. Giani, S. Leroy, C. & Rancoita, P.G. (Singapore: World Scientific), 513–518
- Chang, J., et al., 2008, *Nature*, 456, 362–365
- Cirelli, M. & Cline, J.M., 2010, *Phys. Rev. D*, 82, 023503
- Clem, J.M. & Dorman, L.I., 2000, *Space Sci. Rev.*, 93, 335–359
- Clem, J.M. et al., 1996, *ApJ*, 464, 507–515
- Clem, J.M. et al., 2000, *J. Geophys. Res.*, 105(A10), 23099–23105
- Clover, E. W. & Ling, A.G., 2001, *ApJ*, 551, L189–L192
- Emerson, P. & Meyer, P., 1984, *J. Geophys. Res.*, 89, 2647–2654
- Evoli, C., Gaggero, D., Grasso, D. & Maccione, L., 2008, *J. Cosmology Astropart. Phys.*, 10, 018
- Ferreira, S.E.S. et al., 2003, *Ann. Geophys.*, 21, 1359–1366
- Ferreira, S.E.S. & Potgieter, M.S., 2003, *Adv. in Sp. Res.*, 32, 657
- Ferreira, S.E.S. & Potgieter, M.S., 2004, *ApJ*, 603, 744–752

- Ferreira, S.E.S., Potgieter, M.S., Burger, R.A., Heber, B. and Fichtner, H., 2001, 106(A11), 24979–24987
- Fichtner, H., Sreenivasan, S.R., Fahr, H.J., 1996, A&A, 308, 248–260
- Fisk, L.A., 1976, J. Geophys. Res., 81, 4646–4650
- Fisk, L.A., 1996, J. Geophys. Res., 101, 15547–15554
- Garcia-Munoz, M., Meyer, P., Pyle, K.R. & Simpson, J.A., 1986, J. Geophys. Res., 91(A3), 2858–2866
- Gardiner, C.W., 1985, Handbook of stochastic methods: for physics, chemistry and natural sciences (Springer Edition)
- Gervasi, M., Rancoita, P.G., Usoskin, I.G., & Kovaltsov, G.A., 1999, Nucl. Phys. B, Proc. Suppl., 78, 26–31
- Giacalone, J., 1998, Space Sci. Rev., 83, 351–363
- Giacalone, J. & Jokipii, J.R., 1999, ApJ, 520, 204–214
- Gleeson, L.J. & Axford, W.I., 1968, ApJ, 154, 1011–1026
- Gleeson, L.J. & Urch, I.H., 1971, Ap&SS, 11, 288–308
- Gleeson, L.J. & Urch, I.H., 1973, Ap&SS, 25, 387–404.
- Gloeckler, G. & Jokipii, J.R., 1966, Phys. Rev. Lett., 17, 203–207
- Haino, S. et al., 2004, Phys. Lett. B, 594, 35–46
- Haasbroek, L.J., & Potgieter, M. S., 1995, Space Sci. Rev., 72, 385–390
- Hattingh, M. & Burger, R.A., 1995, Adv. Space Res., 16, 213–216
- Heber, B., Bothmer, V., Dröge, W., et al., 1998, J. Geophys. Res., 103 (A3), 4809–4816
- Heber, B., Gieseler, J., Dunzlaff, P., Gmez-Herrero, R., Klassen, A., Mller-Mellin, R., Mewaldt, R.A., Potgieter, M.S., Ferreira, S.E.S.. 2008, ApJ, 689(2), 1443–1447
- Herbst, K., Kopp, A., Heber, B., Steinhilber, F., Fichtner, H., Scherer, K. & Matthiä, D., 2010, J. Geophys. Res., 115, D00I20
- Hitge, M. & Burger, R.A., 2010, Adv. Space Res., 45, 18–27

- Hoeksema, J.T., 1995, *Space Sci. Rev.*, 72, 137–148
- Ibarra, A., Tran, D. & Weniger, C., 2010, *J. Cosmology Astropart. Phys.*, 01, 009
- Isenberg, P.A. & Jokipii, J.R., 1979, *ApJ*, 234, 746–752
- Jokipii, J.R., 1971, *Rev. Geophys. Space Phys.*, 9, 27–87
- Jokipii, J.R. & Kota, J., 1989, *Geophys. Res. Lett.*, 16, 1–4
- Jokipii, J.R. & Kóta, J., 1995, *Space Sci. Rev.*, 72, 379–384
- Jokipii, J.R. & Parker, N.E., 1970, *ApJ*, 160, 735–744
- Jokipii, J.R. & Levy, E.H., 1977, *ApJ*, 213, L85–L88
- Jokipii, J.R. & Thomas, B., 1981, *ApJ*, 243, 1115–1122
- Jokipii, J.R., Levy, E.H. & Hubbard, W.B., 1977, *ApJ*, 213, 861–868
- King, J.H. & Papatashili, N.E., 2005, *J. Geophys. Res.*, 110, A02104; Solar wind and IMF Magnitude Average data as extracted from NASA/GSFC’s OMNI data set through OMNIWeb at the website: <http://omniweb.gsfc.nasa.gov/form/dx1.html>
- Kóta, J. & Jokipii, J.R., 1989, *Geophys. Res. Lett.*, 16, 1–4
- Kruells, W.M. & Achterberg, A., 1994, *A&A*, 286, 314–327
- Langner, U.W., 2004, Ph.D. Thesis, Potchestroom University, Potchestroom.
- Langner, U.W., Potgieter, M.S. & Webber, W.R., 2003, *J. Geophys. Res.*, 108, 8039
- Langner, U.W. & Potgieter, M.S., 2004, *J. Geophys. Res.(Space Physics)*, 109, 1103
- Langner, U.W. & Potgieter, M.S., 2005, *ApJ*, 630, 1114–1124
- Leroy, C. & Rancoita, P.G. 2007, *Rep. Prog. in Phys.*, 70, 493–625
- Leroy, C. & Rancoita, P.G. 2011, *Principles of Radiation Interaction in Matter and Detection* - 3rd Edition (Singapore: World Scientific), ISBN: 978-981-4360-51-7
- Lockwood, J.A. & Webber, W.R. 2000, *J. Geophys. Res.*, 104, 24845–24862
- Mc Comas, D.J. et al., 2000, *J. Geophys. Res.*, 105, 10419–10434
- Menn, W. et al., 2000, *ApJ*, 533, 281–297

- Mertsch, P. & Sarkar, S., 2011, Proc. of the 12th ICATPP Conference on Cosmic Rays for Particle and Astroparticle Physics, ed. Giani, S. Leroy, C. & Rancoita, P.G. (Singapore: World Scientific), 535–543
- Meyer-Vernet, N., 2007, Basics of the Solar Wind,(Cambridge: Cambridge University Press)
- Mitchell, J.W. et al., 2008, Proc. of the 30th ICRC, ed. R. Caballero, J.C. D’Olivo, G. Medina-Tanco, L. Nellen, F. A. Snchez & J. F. Valds-Galicia (Mexico City), 455–458
- Moskalenko, I.V., Strong, A.W., Hormes, J.F. & Potgieter, M.S., 2002, ApJ, 656, 280–296
- Ndiitwani, D.C. et al., 2005, Ann. Geophys., 23, 1061–1070
- Palmer, I.D., 1982. Rev. Geophys., 20, 335–351
- Parker, E.N., 1957, Phys. Rev., 107, 924–933
- Parker, E.N., 1958, ApJ, 128, 664
- Parker, E.N., 1965, Planet. Space Sci., 13, 9
- Pei, C., Bieber, J.W., Breech, B., Burger, R.A., Clem, J., Matthaeus, W.H., 2010a, J. Geophys. Res., 115, A03103
- Pei, C., Bieber, J. W., Burger, R. A. & Clem, J., 2010b, J. Geophys. Res., 115, A12107
- Pei, C., Bieber, J.W., Burger, R.A. & Clem, J., 2010c, Journal of Geophysical Research (Space Physics), 115, 12107
- Perko, J.S., 1987, A&A, 184, 119–121
- PDB (2010): Nakamura, K. et al. (Particle Data Group), 2010. Review of Particle Physics, J. Phys. G, 37, 075021; the latest versions of tables, reference data and constants are available at the Particle Data Group web site: <http://pdg.lbl.gov/pdg.html>
- Pommois, P., Zimbardo, G. & Veltri, P., 2001, Nonlin. Proc. in Geophy., 8, 151–158
- Potgieter, M.S., 1995, Ap&SS, 230, 393
- Potgieter, M.S., 1997, Proc. 25th ICRC, ed.M. S. Potgieter, C. Raubenheimer & van der Walt, D.J., 1
- Potgieter, M.S., 1998, Space Sci. Rev., 83, 147–158.
- Potgieter, M.S., 2000, J. Geophys. Res., 105, 18295–18304

- Potgieter, M.S., 2008, *J. of Atmosph. and Solar-Terr. Phys.*, 70, 207–218
- Potgieter, M.S., Burger, R.A. & Ferreira, S.E.S., 2001, *Space Sci. Rev.*, 97, 295–307
- Potgieter, M.S. & Ferreira, S.E.S., 2001, *Adv. in Sp. Res.*, 27, 481–492
- Potgieter, M.S. & Ferreira, S.E.S., 2002, *J. Geophys. Res.*, 107, A7, 1089
- Potgieter, M.S., Ferreira, S.E.S. & Heber, B., 2003, *Adv. in Sp. Res.*, 32, 645–650
- Potgieter, M.S., Le Roux, J.A. & Burger, R.A., 1989, *J. Geophys. Res.*, 94, 2323
- Potgieter, M.S. & Le Roux, J.A., 1994, *ApJ*, 423, 817
- Potgieter, M.S., Le Roux, J.A., Burlaga, L.F. & McDonald, F.B., 1993, *ApJ*, 403, 760–768
- Potgieter, M.S. & Moraal, H., 1985, *ApJ*, 294, 425–440
- Putze, A., Derome, L., Maurin, D., Perotto, L. & Taillet, R., 2009, *A&A*, 497, 991–1007
- Ruždjak, D., Brajša, R., Sudar, D. & Wölf, H., 2005, *Sol. Phys.*, 229, 35–43
- Salati, P., 2011, *Proc. of the 12th ICATPP Conference on Cosmic Rays for Particle and Astroparticle Physics*, ed. Giani, S. Leroy, C. & Rancoita, P.G. (Singapore: World Scientific), 613–625
- Sanderson, T.R., Appourchaux, T., Hoeksema, J. T. & Harvey, K.L., 2003, *J. Geophys. Res.(Space Physics)*, 108, SSH 7-1
- Sanuki, T. et al., 2000, *ApJ*, 545, 1135–1142
- Shikaze, Y. et al., 2007, *Astropart. Phys.*, 28, 154–167
- Simpson, J.A., 1992, *Astron. Astrophys. Suppl. Ser.*, 92(2), 365-399.
- Simpson, J.A., 1996, *Nuov. Cim. C*, 19C, 935–943
- Simpson, J.A., Zhang, M., Bame, S., 1996, *ApJ*, 465, L69
- SSN, see the web site at: <http://www.sidc.oma.be/sunspot-data/>
- Stone, E.C., Cummings, A.C., McDonald, F.B., Heikkila, B.C., Lal, N. & Webber, W.R., 2005, *Science*, 309, 2017–2020
- Stone, E.C., Cummings, A.C., McDonald, F.B., Heikkila, B.C., Lal, N. & Webber, W.R., 2008, *Nature*, 454, 71–74

- Strauss, R.D., Potgieter, M.S., Busching, I. & Kopp, A., 2011, *ApJ*, 735, 83
- Strong, A.W. & Moskalenko, I.V., 2004, *ApJ*, 613, 962–976
- Strong, A.W., Moskalenko, I.V., & Ptuskin, V.S., 2007, *Ann. Rev. Nuclear and Particle Sci.*, 57, 285–327
- Trotta, R. et al., 2011, *ApJ*, 729, 106
- Usoskin, I.G., Alanko, K., Mursula, K. & Kovaltsov, G.A., 2002, *Sol. Phys.*, 207, 389–399.
- Usoskin, I.G. et al., 2005, *J. Geophys. Res.*, 110, A12108
- Yamada Y., Yanagita S. & Yoshida T., 1998, *Geophys. Res. Lett.*, 25, 2353–2356
- Wang, Y.-M. & Sheeley, N. R., 2002, *J. Geophys. Res.(Space Physics)*, 107, SSH 10-1
- Whang, Y.C. & Burlaga, L.F., 2000, *Geophys. Res. Lett.*, 27, 1607–1610
- Whang, Y.C., Burlaga, L.F., Wang, Y.-M. & Sheeley, N.R., 2003, *ApJ*, 589, 635–643
- Whang, Y.C., Burlaga, L.F., Wang, Y.-M. & Sheeley, N.R., 2004, *Geophys. Res. Lett.*, 31, L03805
- Webber, W.R., Cummings, A.C., Mc Donald, F.B., Stone, E.C., Heikkila, B., Lal, N., 2008, *J. Geophys. Res.*, 113, A10108
- Weniger, C., 2011, *Proc. of the 12th ICATPP Conference on Cosmic Rays for Particle and Astroparticle Physics*, ed. Giani, S. Leroy, C. & Rancoita, P.G. (Singapore: World Scientific), 632–640
- Wenzel, K.-P., Marsden, R.G., Page, D.E. & Smith, E.J., 1992, *Astron. Astrophys. Suppl. Ser.*, 92, 207
- Wibberenz, G., Ferreira, S.E.S., Potgieter, M.S. & Cane, H.V., 2001, *Space Sci. Rev.*, 97, 373–376
- WSO, 2010, see the web site:
<http://wso.stanford.edu/Tilts.html>
- Zhang, M., 1999, *ApJ*, 513, 409–420

